Received: 8 July 2021 | Revised: 15 April 2022 | Accepted: 10 June 2022

DOI: 10.1111/bph.15910

RESEARCH ARTICLE

Riociguat attenuates the changes in left ventricular proteome and microRNA profile after experimental aortic stenosis in mice

Alexander Benkner[1,2] | Julia Rüdebusch[1,2] | Neetika Nath[3] | Elke Hammer[1,4] | Karina Grube[1,2] | Stefan Gross[1,2] | Vishnu M. Dhople[1,4] | Gertrud Eckstein[5] | Thomas Meitinger[5,6] | Lars Kaderali[1,3] | Uwe Völker[1,4] | Jens Fielitz[1,2] | Stephan B. Felix[1,2]

[1]German Centre for Cardiovascular Research (DZHK), Greifswald, Germany

[2]Department of Internal Medicine B, Cardiology, University Medicine Greifswald, Greifswald, Germany

[3]Institute of Bioinformatics, University Medicine Greifswald, Greifswald, Germany

[4]Interfaculty Institute for Genetics and Functional Genomics, University Medicine Greifswald, Greifswald, Germany

[5]Institute of Human Genetics, Helmholtz Centre Munich, Neuherberg, Germany

[6]German Centre for Cardiovascular Research (DZHK), partner site Munich Heart Alliance, Munich, Germany

Correspondence
Stephan B. Felix, Department of Cardiology and Internal Medicine B, University Medicine Greifswald, Ferdinand-Sauerbruch-Strasse, 17475 Greifswald, Germany.
Email: felix@uni-greifswald.de

Funding information
Deutsches Zentrum für Herz-Kreislaufforschung (DZHK), Grant/Award Number: 81Z5400153

Background and Purpose: Development and progression of heart failure involve endothelial and myocardial dysfunction as well as a dysregulation of the NO-sGC-cGMP signalling pathway. Recently, we reported that the sGC stimulator riociguat has beneficial effects on cardiac remodelling and progression of heart failure in response to chronic pressure overload. Here, we examined if these beneficial effects of riociguat were also reflected in alterations of the myocardial proteome and microRNA profiles.

Experimental Approach: Male C57BL/6N mice underwent transverse aortic constriction (TAC) and sham-operated mice served as controls. TAC and sham animals were randomised and treated with either riociguat or vehicle for 5 weeks, starting 3 weeks after surgery, when cardiac hypertrophy was established. Afterwards, we performed mass spectrometric proteome analyses and microRNA sequencing of proteins and RNAs, respectively, isolated from left ventricles (LVs).

Key Results: TAC-induced changes of the LV proteome were significantly reduced by treatment with riociguat. Bioinformatics analyses revealed that riociguat improved TAC-induced cardiovascular disease-related pathways, metabolism and energy production, for example, reversed alterations in the levels of myosin heavy chain 7, cardiac phospholamban and ankyrin repeat domain-containing protein 1. Riociguat also attenuated TAC-induced changes of microRNA levels in the LV.

Conclusion and Implications: The sGC stimulator riociguat exerted beneficial effects on cardiac structure and function during pressure overload, which was accompanied by a reversal of TAC-induced changes of the cardiac proteome and microRNA profile. Our data support the potential of riociguat as a novel therapeutic agent for heart failure.

List of abbreviations: CVD, cardiovascular disease; HF, heart failure; HFpEF, heart failure with preserved ejection fraction; HFrEF, heart failure with reduced ejection fraction; LV, left ventricle; NO, nitric oxide; RIO, riociguat; sGC, soluble guanylyl cyclase; TAC, transverse aortic constriction; VEH, vehicle.

KEYWORDS
cardiac remodelling, heart failure, microRNA sequencing, proteomics, riociguat, soluble guanylyl cyclase stimulator, TAC

1 | INTRODUCTION

Heart failure (HF) is associated with high morbidity and mortality despite the use of pharmacological and instrumental interventions (Linden et al., 2020). Whereas no evidence-based treatment is available to improve the prognosis of HF with preserved ejection fraction (HFpEF), drug treatment reduces the morbidity and mortality in HF with reduced ejection fraction (HFrEF) (Ponikowski et al., 2016). Despite considerable advances in therapy, the prognosis of HFrEF is still poor (Murphy et al., 2020). Regardless of the underlying cause of HFrEF, there are structural, metabolic and molecular changes in the left ventricular myocardial tissue. To counteract these pathological changes and to improve the progression of HF, new therapies are needed (Bernardo et al., 2010). Myocardial and endothelial dysfunctions are involved in the development and progression of HF and dysregulation of several signalling pathways, including the **nitric oxide (NO)–soluble guanylyl cyclase (sGC)–cyclic guanosine monophosphate (cGMP)** signalling pathway (NO-sGC-cGMP), contributes to these processes (Stasch et al., 2011). NO is produced by the **endothelial NO synthase (eNOS)** and acts as an important signalling molecule: In vascular smooth muscle cells (SMC), NO activates sGC that catalyses the synthesis of the second messenger cGMP thus regulating various physiological processes and tissue-protective effects, including smooth muscle relaxation, inhibition of inflammation, SMC proliferation and platelet activation (Mitrovic et al., 2011). In HF, reactive oxygen species (ROS) and inflammatory mediators reduce NO bioavailability (Umar & van der Laarse, 2010). Reduction of NO bioavailability and an altered redox state of sGC, which makes the enzyme insensitive to NO, lead to an impairment of the NO-sGC-cGMP pathway. A reduced sGC activity causes cGMP deficiency that is associated with cardiac hypertrophy, interstitial fibrosis, vasoconstriction and platelet aggregation (Shah et al., 2018; Umar & van der Laarse, 2010). A restoration of the NO-sGC-cGMP pathway may therefore have cardioprotective effects in HF patients. Promising substances in this regard are NO-independent but haem-dependent sGC stimulators (Mittendorf et al., 2009). Those compounds directly stimulate sGC in the absence of NO and sensitise sGC to low levels of NO (Stasch & Hobbs, 2009). Agonists of sGC could have beneficial effects in HFrEF by smooth muscle relaxation and vasodilation, thereby decreasing right and left ventricular afterload (Stasch et al., 2011). Previous studies focused on the use of sGC stimulators in preclinical models of cardiovascular disease (CVD) and suggested that sGC stimulators might prevent cardiac dysfunction and HF independently of their haemodynamic effects (Sandner, 2018). One of these drugs is **riociguat** (BAY 63-2521). Recently, we reported that riociguat reduced left ventricular contractile failure, remodelling, hypertrophy, fibrosis and inhibited the expression of myocardial stress and remodelling genes in a mouse model of increased afterload caused by transverse aortic constriction (TAC) (Rüdebusch et al., 2020). Here, we extend our previous study and provide new insights into the effects of riociguat on the proteome and microRNA transcriptome of the left ventricle (LV) of TAC-induced HF.

What is already known

- Heart failure is associated with impaired NO-sGC-cGMP signalling.
- sGC stimulators may serve as novel therapeutic agents in heart failure.

What does this study add

- Riociguat improves cardiac structure and function in a mouse model of heart failure.
- These improvements were accompanied by attenuated TAC-induced changes of the cardiac proteome and microRNA profile.

What is the clinical significance

- Our data provides new insights into molecular changes induced by sGC stimulation in heart failure.
- Our findings support the potential of riociguat as a novel therapeutic agent for heart failure.

2 | METHODS

A more detailed description of methods is available in the Supporting Information.

2.1 | Ethical statement

All animal care and experimental procedures were in accordance with Directive 2010/63/EU of the European Parliament and of the Council of 22 September 2010 on the protection of animals used for scientific

purposes and were approved by the local animal care committee (Landesamt für Landwirtschaft, Lebensmittelsicherheit und Fischerei Mecklenburg-Vorpommern; LALLF MV, 7221.3–1–006/16). Animal studies are reported in accordance with the ARRIVE guidelines (Percie du Sert et al., 2020) and the British Journal of Pharmacology recommendations (Lilley et al., 2020).

2.2 | Study design, experimental set-up and sample generation

All animal experiments were performed as previously described and samples from the same animals were used for analyses of the present study (Rüdebusch et al., 2020). In brief, 8-week-old male C57BL/6N wild-type mice (Charles River Laboratories, Sulzfeld, Germany, RRID:MGI:5651595) underwent either TAC or sham surgery. Initial anaesthesia was performed with 3% isoflurane, followed by intubation and ventilation (2% isoflurane in air at 50 ml·min^{-1}) for surgery. Animals were treated with buprenorphine (s.c., 0.02 mg·kg^{-1} body weight) as analgesic medication before and for 3 days (every 12 h) after surgery with daily monitoring until the end of the study. At Day 21, mice were randomly assigned to be treated with riociguat (Adempas®: BAY 63-2521; 3 mg·kg^{-1} body weight per day) or vehicle (VEH, Transcutol®/Cremophor®/water: 10/20/70%), resulting in four treatment groups ($n = 5$–6 per group): sham + vehicle ($Sham_{/VEH}$), sham + riociguat ($Sham_{/RIO}$), TAC + vehicle ($TAC_{/VEH}$) and TAC + riociguat ($TAC_{/RIO}$). Riociguat or vehicle were administered by daily oral gavage for five more weeks. During all animal procedures and throughout the entire animal protocol, we assessed the health status of the animals. A predefined scoring system that was approved by the animal welfare authorities and our local veterinarian was used to achieve humane endpoints. The scoring system included (1) appearance, (2) respiration, (3) weight loss, (4) spontaneous behaviour, (5) provoked behaviour and (6) abdominal palpation. Each parameter was monitored daily for the entire duration of the study and was scored from 0 (normal) to 3 (strongly deteriorated). A humane endpoint was reached if either one criterion scored 3 or a sum score of ≥9 was reached and such animals were killed by cervical dislocation. At the end of the experiment, at Day 56, mice were given an overdose of thiopental (i.p., 300 mg·kg^{-1} body weight) followed by retrograde perfusion through the abdominal aorta with ice-cold PBS and removal of hearts. The LV free walls were dissected, snap-frozen and stored at −80°C until further use.

2.3 | Sample preparation for proteomics and microRNA sequencing

The snap-frozen LV tissue was coarsely grounded into powder and equally divided into two parts, one for protein and one for RNA/microRNA extraction. The tissue powder was further disrupted using a Mikro-Dismembrator (Sartorius, Göttingen, Germany) at 2600 rpm for 2 min. For protein extraction, samples were dissolved in 8 M urea/2 M thiourea (UT). Lysates were three times sonicated on ice for 5 s with nine cycles at 80% energy using a Sonopuls (Bandelin, Berlin, Germany). After centrifugation at 16,000 × g for 1 h, the protein-containing supernatants were stored at −80°C until further use. Protein concentrations were determined using Bradford reagent (Bio-Rad, Munich, Germany). For RNA and microRNA preparation, samples were dissolved in QIAzol® (QIAGEN, Hilden, Germany). RNA was isolated using miRNeasy Mini Kit (QIAGEN), and RNA quality and concentration were assessed using Agilent RNA 6000 Nano Kit according to the manufacturer's instructions. Samples were allocated blindly and randomly selected for sample preparation and processing.

2.4 | Proteome analysis

2.4.1 | Sample preparation

Proteome analysis was performed on proteins isolated from LV of five to six mice from each experimental group. Proteins were reduced with dithiothreitol (2.5 mM, 60°C, 1 h) and alkylated with iodoacetamide (10 mM, 37°C, 30 min). Then, LysC digestion (10 ng per 1 μg protein) at 37°C for 3 h was followed by trypsin digestion (100 ng per 1 μg protein) at 37°C for 16–18 h. Acetic acid was added to a final concentration of 1%, to stop the digestion. The resulting peptides were cleaned using reversed-phase material (μ-C18 ZipTips, Millipore, Billerica, MA, USA) and subjected to liquid chromatography (LC)–electrospray ionisation (ESI)–tandem mass spectrometry (MS/MS). The experimenter was blinded to sample allocation, and MS/MS measurements of randomly assigned samples were conducted.

2.4.2 | LC-ESI-MS/MS

Separation of peptides was performed on a nanoAquity UPLC system (Waters Corporation, Manchester, UK) on C18 reversed-phase material in a non-linear 88 min gradient of 5% to 60% ACN in 0.1% acetic acid (flow: 400 nl·min^{-1}). The detection of eluting peptides was carried out with a LTQ-Orbitrap-Velos mass spectrometer (Thermo Fisher Scientific, Bremen, Germany) in data-dependent mode (Rüdebusch et al., 2017). The mass spectrometry proteomics data have been deposited to the ProteomeXchange (RRID:SCR_004055) Consortium via the PRIDE (Perez-Riverol et al., 2019) partner repository with the dataset identifier PXD024156.

2.4.3 | Database search, identification and quantification

Peptides and proteins were identified via a MaxQuant search (version 1.5.3.8, RRID:SCR_014485) in a murine UniProt/Swiss-Prot database (rel. 02/22/2017, RRID:SCR_002380). For protein identification and label free quantification, razor and unique peptides were included (peptides ≥1). For quantification and further downstream analyses the normalised protein intensities (LFQ values) calculated by MaxLFQ, a completely into MaxQuant integrated software algorithm, were

extracted (Cox et al., 2014). LFQ values were imported into the Genedata® Analyst™ software (version 10.0.3, Genedata®, Basel, Switzerland, RRID:SCR_021326) and only proteins with at least 50% valid values per group were considered for quantification. In order to also obtain information about the non-quantifiable proteins (<50% valid values), an absent/present search within Genedata® was performed.

2.4.4 | Functional classification

Functional classification of significantly altered proteins was performed using Ingenuity Pathway Analysis (IPA®, RRID:SCR_008653). To evaluate and identify the direction of affected biological processes, downstream effects analyses (DEA) were conducted. The correlation between relationship and direction was predicted based on IPA's *z*-score algorithm. A downstream effect *z*-score ≥2 or ≤−2 was considered significant, indicating activation ($z \geq 2$) and inhibition ($z \leq -2$) of biological function, respectively (Kramer et al., 2014).

2.4.5 | Western blot analysis

For immunoblotting and according to manufacturer's protocol, TGX Stain-Free™ FastCast™ acrylamide gels (Bio-Rad, Hercules, CA, USA) were used for in-gel protein labelling and later normalisation to total protein (Gürtler et al., 2013). Primary antibodies recognising ankyrin repeat domain-containing protein 1 (Abcam, Cat# ab64963, RRID:AB_1140785), myosin heavy chain 7 (Abcam, Cat# ab172967, RRID:AB_2892244), phospholamban (Abcam, Cat# ab2865, RRID:AB_2167905) and phosphorylated phospholamban (Ser16) (Abcam, Cat# ab15000, RRID:AB_301562) were used (for details, see Supporting Information).

2.5 | MicroRNA sequencing analysis

2.5.1 | Sample preparation and sequencing

One microgram of total RNA per sample ($n = 6$ per group) was used for microRNA library construction using the TruSeq® small RNA Library Preparation Kit (Illumina, San Diego, CA, USA) according to the manufacturer's protocol. Libraries were sequenced as 100 bp paired-end runs on one lane, respectively, on an Illumina HiSeq® 4000 platform. Samples were handled in a blinded fashion during library preparation and sequencing process.

2.5.2 | Bioinformatics pipeline

For bioinformatics data analysis, software packages available on R-CRAN (RRID:SCR_001905) or Bioconductor (RRID:SCR_006442) were used. Furthermore, Trimmomatic package (version 0.35, RRID:SCR_011848) and FASTQC (version 0.11.9, RRID:SCR_014583) was used for data quality assessment. Next, miRDeep2 (version 0.1.2, RRID:SCR_010829) was used for identification of known microRNAs with the bowtie package (version 1.2.3, RRID:SCR_005476) for alignment with the miRBase database (version 22.1, RRID:SCR_003152) (An et al., 2013). DESeq2 (version 1.32.0, RRID:SCR_015687) was further taken to compute differential expression (Love et al., 2014). In addition to known microRNAs, miRDeep2 also identifies novel and unknown microRNAs with high estimates. Based on their scores, the novel microRNAs were selected (Bonnet et al., 2004). All microRNA-Seq fastq data are available at the Sequence Read Archive (RRID:SCR_004891) (BioSample accession: SAMN17674846 and BioProject: PRJNA697862).

2.5.3 | Functional classification

Analysis of microRNA-pathway association was performed using the Pathway Dictionary Database (miRPathDB v2.0, RRID:SCR_017356) and was based on the *Mus musculus* reference genome ver 2020-07-15 (Kehl et al., 2020). To perform microRNA-to-pathway enrichment analysis, GeneTrail2 (RRID:SCR_006250) library was used (Stöckel et al., 2016). Pathways were taken from the Kyoto Encyclopaedia of Genes and Genomes (KEGG, RRID:SCR_012773), and microRNA annotations were considered from miRBase. Further, IPA®'s microRNA target filter was used to identify putative microRNA target genes. To reveal the effects of microRNAs on the proteome profile, proteomic and microRNA datasets were integrated and analysed to identify inverse expression patterns. Here, targets filtered for CVD-related associations and heart tissue specificity were taken into account in particular.

2.5.4 | Validation of key microRNAs by qPCR

Using the miRCURY LNA RT Kit (QIAGEN) microRNAs were reverse transcribed from total RNA, followed by quantitative real-time PCR (qPCR) using the miRCURY LNA SYBR® Green PCR Kit (QIAGEN) and individual miRCURY LNA miRNA PCR Assays (QIAGEN) for a subset of 22 key microRNAs according to manufacturer's protocol. Detailed primer information regarding the miRNA PCR Assays can be found in the Supporting Information. The expression of microRNA was normalised to the geometric mean of three stably expressed microRNAs (i.e., mmu-let-7a-5p, mmu-miR-16-5p, mmu-miR-191-5p) identified from the microRNA-Seq data as suitable reference genes and following the manufacturer's instructions from QIAGEN's miRCURY LNA miRNA SYBR® Green PCR Handbook. All qPCR-related experiments were performed by experimenters who were blinded to samples' information. For relative quantification of expression levels the $2^{-\Delta\Delta Ct}$ method was used (Livak & Schmittgen, 2001).

2.6 | Data and statistical analysis

The data and statistical analysis comply with the recommendations on experimental design and analysis in pharmacology (Curtis et al., 2018). All statistical tests of LC-ESI-MS/MS data were carried out in

Genedata® Analyst™ (version 10.0.3, Genedata®, Basel, Switzerland, RRID:SCR_021326) with $\log_{10}$-transformed LFQ values. Differentially abundant proteins were identified by comparing corresponding groups ($TAC_{/VEH}$ vs. $Sham_{/VEH}$, $TAC_{/RIO}$ vs. $Sham_{/RIO}$, $TAC_{/RIO}$ vs. $TAC_{/VEH}$ and $Sham_{/RIO}$ vs. $Sham_{/VEH}$) using a Welch's *t*-test. Proteins identified with at least two peptides and with $P < 0.05$ were considered as significantly different between treatment groups. Significance of the enrichment of proteins among functional categories was assessed via Fisher's exact test. Western blot and qPCR results were tested with a Student's *t*-test using GraphPad Prism (version 8.3.0, RRID:SCR_002798). All *P* values less than 0.05 were considered statistically significant. For statistical analysis of microRNA-Seq data, the Wald statistics, that is included in the DESeq2 package, was used for identification of significant differences between two conditions (Chen et al., 2011). Benjamini–Hochberg correction was used in order to compute adjusted *P* values (*q* values). For each pair of microRNA and functional category, a hypergeometric test was applied to test the significance of the determined microRNA-to-pathway association. The selection of significant associations was carried out at a significance level of FDR < 0.05. One-tailed Pearson correlation analyses among variables of $\log_2$-transformed microRNA-Seq counts and corresponding MS protein intensities of putative mRNA targets were performed on single sample level for $TAC_{/VEH}$ and $TAC_{/RIO}$ using GraphPad Prism (version 8.3.0, RRID:SCR_002798).

2.7 | Materials

Riociguat and buprenorphine were supplied by Bayer (Leverkusen, Germany); isoflurane was supplied by CP-Pharma (Burgdorf, Germany) and transcutol and cremophor by Sigma-Aldrich (St. Louis, MO, USA).

2.8 | Nomenclature of targets and ligands

Key protein targets and ligands in this article are hyperlinked to corresponding entries in the IUPHAR/BPS Guide to PHARMACOLOGY (http://www.guidetopharmacology.org) and are permanently archived in the Concise Guide to PHARMACOLOGY 2021/22 (Alexander, Fabbro, Kelly, Mathie, Peters, Veale, Armstrong, Faccenda, Harding, Pawson, Southan, Davies, Beuve, et al., 2021; Alexander, Fabbro, Kelly, Mathie, Peters, Veale, Armstrong, Faccenda, Harding, Pawson, Southan, Davies, Boison, et al., 2021).

3 | RESULTS

3.1 | Effects of riociguat treatment on the murine left ventricular proteome after TAC

3.1.1 | Proteomic profiling of LVs across all treatment groups

MS/MS identified 1415 proteins with at least one peptide, and 1127 proteins with two or more peptides were quantified (Figure 1a and Table S1). Principal component analysis (PCA) clearly distinguished sham and TAC mice from each other. The PCA plot also revealed a separate distinct clustering of VEH- and riociguat-treated TAC, but not for both groups of sham mice (Figure S1). To investigate how the LV protein profiles changed after TAC and under riociguat treatment, comparisons of TAC-induced alterations (TAC vs. Sham) with VEH or riociguat were performed. Additionally, riociguat treatment effects (riociguat vs. VEH) in TAC or sham animals were investigated. These analyses revealed that TAC caused strong changes in protein pattern ($TAC_{/VEH}$ vs. $Sham_{/VEH}$: 271 proteins). The TAC-induced changes in protein pattern were less pronounced after riociguat treatment ($TAC_{/RIO}$ vs. $Sham_{/RIO}$: 218 proteins). Interestingly, treatment with riociguat influenced the abundance of only 61 proteins in TAC animals ($TAC_{/RIO}$ vs. $TAC_{/VEH}$) and only 28 proteins in sham animals ($Sham_{/RIO}$ vs. $Sham_{/VEH}$) (Figure 1b). For further analyses, only significantly altered proteins, which were identified with at least two peptides and with a 1.3-fold change (FC) in abundance, were considered unless otherwise stated (Figure 1b, light grey bars). We observed similar proportions of proteins with increased or decreased abundances after TAC in VEH-treated (52 up-regulated, 64 down-regulated) and riociguat-treated animals (33 up-regulated, 26 down-regulated), but a smaller impact of TAC on LV protein levels in riociguat-treated animals (Figure 1b,c). Proteins that showed significant differences in quantity after TAC surgery are mostly localised in the cytoplasm and mitochondria in both VEH- and riociguat-treated animals (Figure 1c and Table S1).

3.1.2 | Functional classification of altered proteins

To investigate the biological pathways and functions affected, a classification of all significantly altered proteins using Ingenuity Pathway Analysis (IPA®) was conducted. Pathways and processes particularly effected by TAC either in combination with or without riociguat treatment are shown in Figure 2. Proteins altered upon TAC were preferentially assigned to pathways related to energy production and metabolism (e.g., *fatty acid β-oxidation* and *oxidative phosphorylation*) and *mitochondrial dysfunction* (Figure 2a). Further, DEA of all significantly altered proteins revealed activation of biological processes such as *degeneration of cells*, *quantity of ROS*, *organ degeneration*, *disorder of lipid metabolism* and *abnormal metabolism* (Figure 2b). Moreover, by assigning these differentially abundant proteins to CVD-related functions, *cardiac dilation*, *fibrosis*, *necrosis/cell death* and *damage* appeared as the strongest affected categories (Figures 2c and S2). Overall, we observed that riociguat attenuated TAC-induced changes of the LV proteome, as indicated by a reduced significance of pathway, process and function enrichment together with fewer altered proteins in riociguat-treated animals.

3.1.3 | Markers of cardiovascular diseases

The attenuation of TAC-induced changes in protein levels by riociguat treatment became even more obvious when significantly different

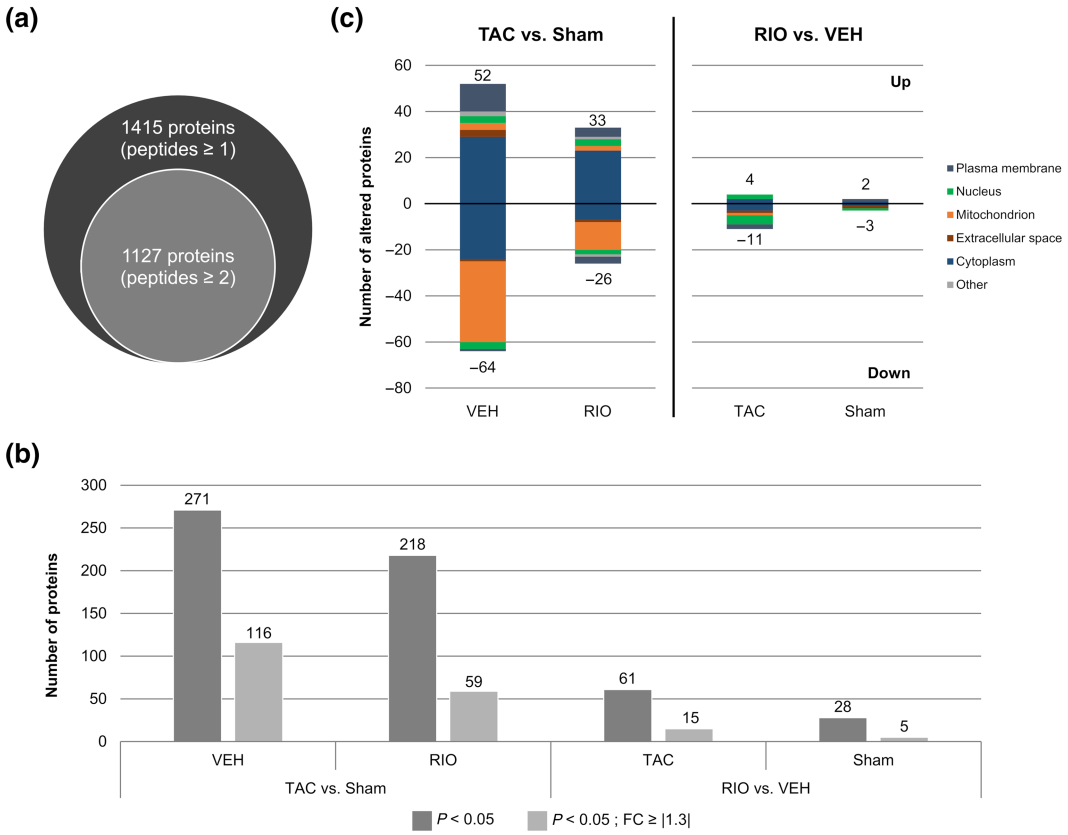

FIGURE 1 Protein identification and alteration in protein levels across all treatment groups. Marked changes in protein abundance in samples of left ventricles (LVs) were observed after transverse aortic constriction (TAC), but less when TAC animals were treated with riociguat (RIO). Changes due to riociguat treatment were comparatively mild. (a) Euler diagram illustrates protein identification in total (dark grey: identifications with at least one peptide) and the protein subset analysed for differential abundance in the four treatment groups (light grey: identification with two or more peptides). (b) Number of identified proteins with significant changes in abundance across the four treatment groups (dark grey: $P < 0.05$ with any fold-change, light grey: $P < 0.05$ and fold-change ≥ |1.3|). (c) Number of altered proteins with at least 1.3-fold change in abundance and their subcellular location is shown. Negative signs indicate numbers of proteins with decreased abundances (proteins identified with ≥2 peptides; $n = 6$, except $Sham_{/VEH} = 5$).

proteins between $TAC_{/VEH}$ versus $Sham_{/VEH}$ assigned to the IPA category of CVD were considered (Figures 3 and S2). This protein set comprised 27 proteins with higher and 19 proteins with lower abundance. Among these proteins, myosin heavy chain 7 (MYH7, $TAC_{/VEH}$ vs. $Sham_{/VEH}$: FC = 19.81) and cardiac phospholamban (PLN, $TAC_{/VEH}$ vs. $Sham_{/VEH}$: FC = −4.37) showed the strongest difference in abundance. TAC-induced CVD-related alterations in the myocardial proteome (e.g., *cardiac damage*, *dilation* and *fibrosis*) were attenuated and partially reversed by riociguat as well (Figures 3a and S2). Likewise, TAC-induced changes of proteins involved in *fatty acid β-oxidation* and *oxidative phosphorylation* were attenuated by riociguat treatment (Figure 3b). Furthermore, an absent/present analysis via Genedata® identified some proteins as selectively present or absent in individual groups (Figure 3c and Table S1). Interestingly, ankyrin repeat domain-containing protein 1 (ANKRD1) was only found in $TAC_{/VEH}$, but not in $Sham_{/VEH}$, $Sham_{/RIO}$ or $TAC_{/RIO}$ mice. To verify these findings, MYH7, PLN and ANKRD1 as representative HF markers were investigated by Western blot (WB) analyses. MS/MS intensities of MYH7 were significantly higher in TAC animals compared to their sham controls and this increase was reduced by riociguat treatment ($TAC_{/RIO}$ compared to $TAC_{/VEH}$; Figure 4a). This finding was confirmed by WB analysis and showed a significant difference between $TAC_{/RIO}$ and $TAC_{/VEH}$ on protein level (Figure 4b). Whereas MS/MS detected ANKRD1 in each sample of the $TAC_{/VEH}$ group, it was not detected in both sham groups and only in two samples of the $TAC_{/RIO}$ group (Figure 3c and Table S1). Again, the data of the WB analysis support the MS/MS results. Significantly increased ANKRD1 levels were observed after TAC, and this increase was significantly reduced by riociguat treatment ($TAC_{/RIO}$ compared to $TAC_{/VEH}$; Figure 4c). For PLN, both MS/MS and WB analyses revealed a decrease of protein levels in $TAC_{/VEH}$, which was attenuated in $TAC_{/RIO}$ (Figure 4a,b). Moreover, because phosphorylation of PLN inhibits its activity on the **sarcoplasmic/endoplasmic reticulum (SR/ER) Ca^{2+}-ATPase (SERCA2a)**, we also investigated its phosphorylation status and found an increased PLN phosphorylation in TAC hearts. We observed a significantly increased ratio of phosphorylated to total PLN (p-PLN/PLN) in $TAC_{/VEH}$ compared to $Sham_{/VEH}$ indicative for additional inhibition of PLN along with reduced abundances of PLN

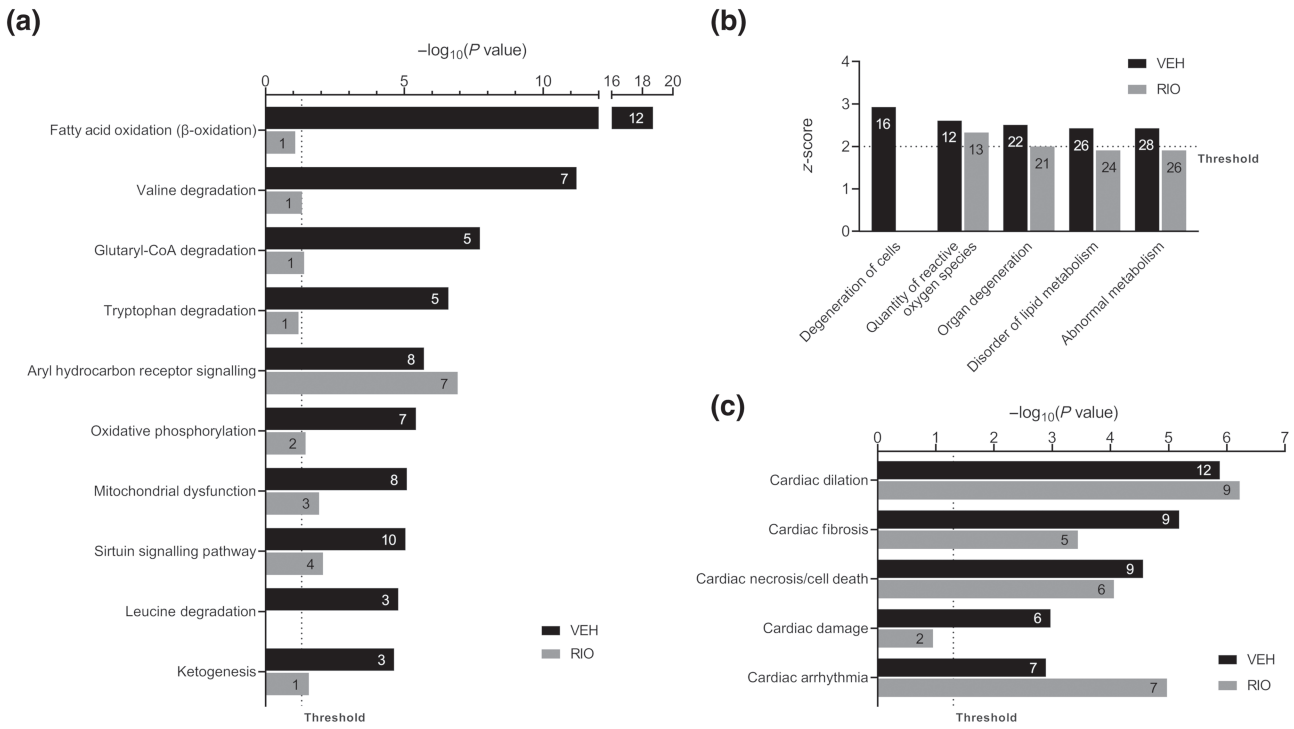

FIGURE 2 Functional classification of left ventricular proteins from TAC vs. sham hearts. Bar graphs represent the significance of over-representation of the functional categories and the number of associated proteins between vehicle (VEH)- and riociguat (RIO)-treated animals. Negative $\log_{10}$-transformed significance values assessed using Fisher's exact test are displayed. (a) Top canonical pathways of significantly altered proteins (≥2 peptides and fold-change ≥ |1.3|) of $TAC_{/VEH}$ and $TAC_{/RIO}$ mice compared to their sham control group are shown. (b) Activation *z*-score analysis of downstream affected biological processes was performed for all differentially abundant proteins (≥2 peptides, $P < 0.05$). *z*-score values represent the predicted direction of regulation where a *z*-score ≥2 indicates significant activation of the biological function. (c) Top 5 CVD-related functional categories of significantly altered proteins (≥2 peptides, $P < 0.05$ and fold-change ≥ |1.3|) are displayed.

(Figure 4b,c). This p-PLN/PLN ratio tended to be reduced after riociguat treatment in $TAC_{/RIO}$, however not reaching significance (Figure 4c).

3.2 | Influence of riociguat treatment on microRNA levels and regulation after TAC

3.2.1 | Identification of differentially expressed microRNAs

Overall, we identified 585 known microRNAs (Table S2). PCA analysis distinguished groups of sham and TAC mice from each other. However, the PCA plot revealed no distinct clustering between VEH- and riociguat-treated groups within the TAC or sham mice (Figure S3). The same group comparisons as for proteomic profiling were set to investigate how the microRNA profiles of LV changed after TAC and under riociguat treatment. A general overview of differentially expressed microRNAs together with their chromosomal localisation in the murine genome is shown in Figure 5. This analysis indicated a higher microRNA expression in both untreated and treated TAC animals compared to their sham controls (Figure 5, inner and middle ring). However, both expression profiles appeared very heterogeneous and differed from each other. Nonetheless, the comparison of $TAC_{/RIO}$ vs. $TAC_{/VEH}$ already showed reversal of changes in microRNA expression, as a result of riociguat treatment after TAC (Figure 5, outer ring). Chromosomes 1, 2, 7, 11, 12 and X seemed to be the hot spots of differential microRNA expression (Figure 5). For further analyses, differentially expressed microRNAs ($q < 0.05$) were considered. Here, substantial differences appeared only when $TAC_{/VEH}$ versus $Sham_{/VEH}$ (43 microRNAs) and $TAC_{/RIO}$ versus $Sham_{/RIO}$ (62 microRNAs) were compared, and similar proportions of up-regulated and down-regulated microRNAs after TAC in VEH-treated (29 up-regulated, 14 down-regulated) and riociguat-treated animals (31 up-regulated, 31 down-regulated) were observed (Figure S4 and Table S3). A subset of relevant altered key microRNAs identified from microRNA-Seq data was validated with qPCR (Figures S5-I and S5-II). In addition, we identified five novel and unknown microRNAs with predicted localisation on chromosomes 1, 2 and 10 (Table S4).

3.2.2 | MicroRNAs-to-pathway analyses

We next performed microRNA-to-pathway association analyses for all 43 microRNAs displaying significantly altered levels after TAC

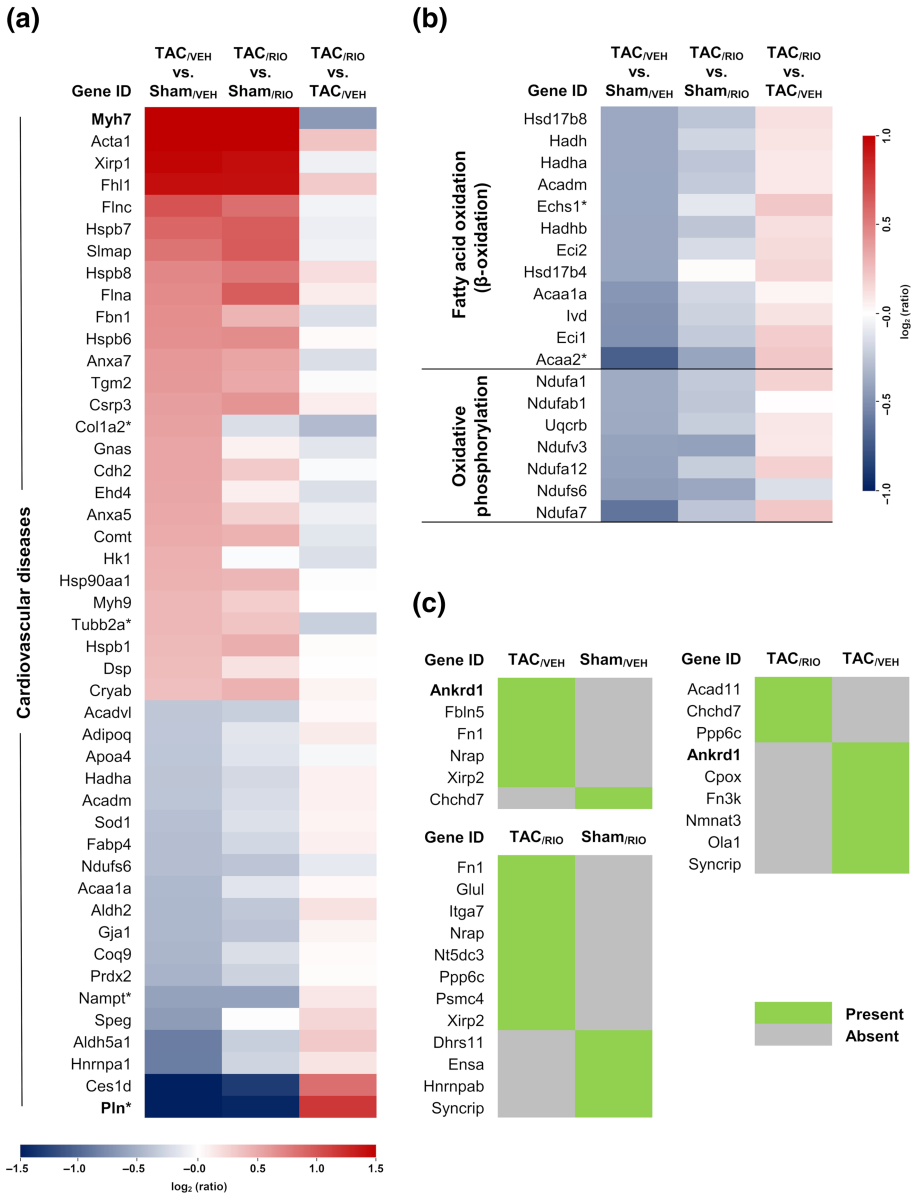

FIGURE 3 Heat maps of proteins significantly altered in abundance after TAC and in response to riociguat (RIO) treatment. Attenuated or partly reversed effects due to riociguat treatment were observed in the protein pattern after TAC surgery. (a) Proteins assigned to the IPA category 'cardiovascular diseases'. (b) Proteins assigned to the IPA categories 'fatty acid β-oxidation' and 'oxidative phosphorylation'. (a,b) The first column displays the $\log_2$ ratio of all proteins with significant changes in abundance due to TAC with FC ≥ |1.3| in vehicle (VEH)-treated animals. Regarding the category-associated proteins, the other columns indicate the respective $\log_2$ ratio from riociguat-treated TAC mice ($TAC_{/RIO}$) compared to riociguat-treated sham mice ($Sham_{/RIO}$) as well as VEH-treated TAC mice ($TAC_{/VEH}$). Red shading denotes an increase and blue shading a decrease within the respective comparison groups. ($^{*}P < 0.05$, significant difference between $TAC_{/RIO}$ and $TAC_{/VEH}$). (c) Proteins were identified regarding their presence (green = present; grey = absent) in treatment and control samples with Genedata's absent/present search.

(Figure 6). Among CVD-related pathways, the most differentially expressed microRNAs were enriched in *adrenergic signalling in cardiomyocytes*, *ErbB signalling* and *cholinergic synapse* (Figure 6). The microRNA associated with most pathways was 'mmu-miR-486a-3p', but it was found to be down-regulated in both riociguat-treated and untreated TAC mice compared to sham controls to almost the same extent and therefore independent of riociguat treatment. With significant up-regulation after TAC, 'mmu-miR-214-3p', 'mmu-miR-27b-3p' and 'mmu-miR-34c-5p' appeared on top of the pathway enrichment lists, suggesting their involvement in regulation of many KEGG pathways. Up-regulation of these three microRNAs was attenuated after riociguat treatment (Figure 6). A variety of microRNAs showed reversed expression patterns related to riociguat treatment, particularly for 'mmu-miR-199a-5p' and 'mmu-miR-208b-3p' in addition to those already mentioned. Interestingly, for almost two thirds (25 microRNAs) of the microRNAs that were differentially regulated by TAC, riociguat attenuated this regulation (Table S3). Additionally, some recently discovered microRNAs that were affected by TAC were reversed by riociguat treatment (e.g., 'mmu-miR-7688-5p', 'mmu-miR-6944-3p' and 'mmu-miR-9769-3p'). Interestingly, 'mmu-miR-122-5p', 'mmu-miR-24-3p', 'mmu-miR-547-3p' and 'mmu-miR-582-3p' showed an increased expression after TAC, and this increase was even higher in riociguat-treated TAC mice. On the other hand, TAC decreased 'mmu-miR-9-5p' and 'mmu-miR-30' expression, which was even more strongly down-regulated in riociguat-treated TAC mice (Figure 6 and Table S3).

3.2.3 | MicroRNA target filter analyses

IPA's microRNA target filter revealed 25 significantly regulated microRNAs in $TAC_{/VEH}$ versus $Sham_{/VEH}$ that showed an inverse expression pairing with 55 putative, CVD-related and heart tissue-specific mRNA targets based on the proteomics dataset (Table S5-I). The same

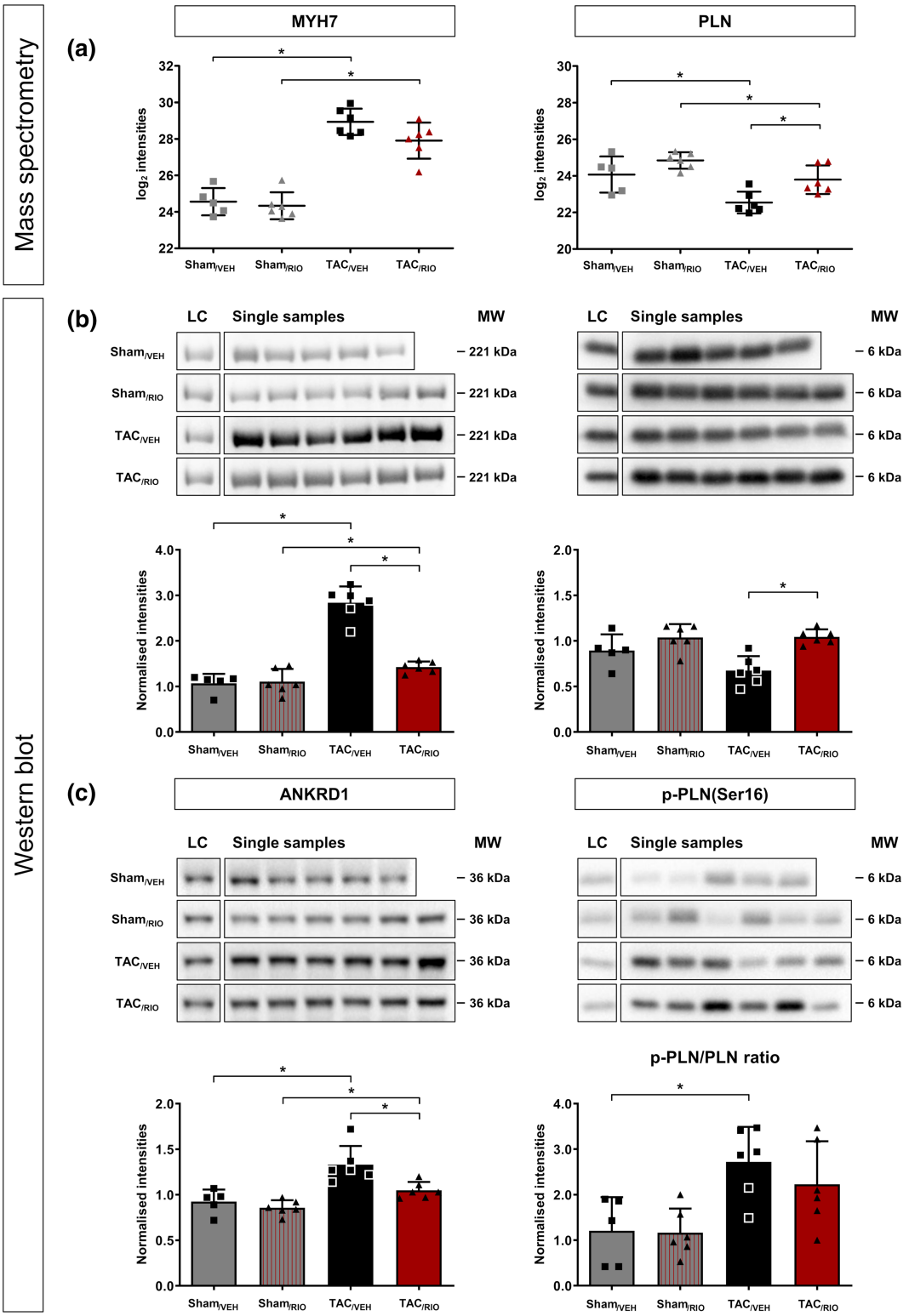

FIGURE 4 Western blot analysis and validation of representative markers of heart failure (HF) found in MS analyses. (a) Normalised and $\log_2$-transformed intensities of MYH7 and PLN from MS; shown with mean ± SD; $n = 6$, except $\text{Sham}_{/VEH} = 5$. $^{*}P < 0.05$, significantly different as indicated; Welch's *t*-test. (b) Corresponding Western blot signals and normalised intensities from Western blots of MYH7 and PLN with mean ± SD; $n = 6$, except $\text{Sham}_{/VEH} = 5$. $^{*}P < 0.05$, significantly different as indicated; Student's *t*-test. (c) Western blot signals and normalised intensities from Western blots of ANKRD1 and p-PLN (p PLN/PLN ratio); shown with mean ± SD; $n = 6$, except $\text{Sham}_{/VEH} = 5$. $^{*}P < 0.05$, significantly different as indicated; Student's *t*-test. (ANKRD1, ankyrin repeat domain-containing protein 1; LC, loading control from pooled $\text{Sham}_{/VEH}$ samples; MYH7, myosin heavy chain 7; MW, molecular weight; PLN, phospholamban; p-PLN, phosphorylated phospholamban (Ser16); SD, standard deviation).

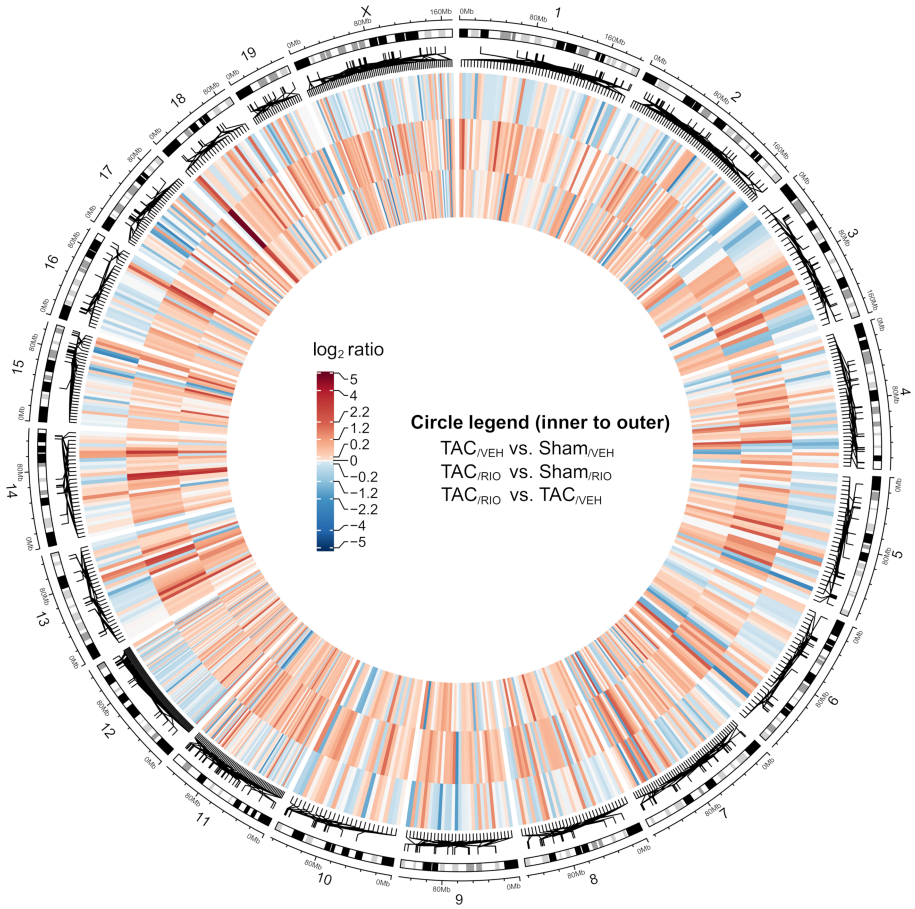

FIGURE 5 Circular heat map for differential expression of microRNAs. General overview of analysed microRNAs and their chromosomal localisation in the murine genome. From inner to outer, the rings display $\log_2$ ratios of microRNAs in three conditions: (1) $TAC_{/VEH}$ versus $Sham_{/VEH}$ (inner), (2) $TAC_{/RIO}$ versus $Sham_{/RIO}$ (middle) and (3) $TAC_{/RIO}$ versus $TAC_{/VEH}$ (outer). Red shading denotes an increase and blue shading a decrease within the respective comparison groups. Reversed microRNA expression due to riociguat (RIO) treatment after TAC was observed (outer ring), despite the heterogeneous expression patterns after TAC compared to sham in RIO-treated (middle ring) and untreated animals (inner ring). Chromosomes 1, 2, 7, 11, 12 and X appear to be the hot spots of microRNA expression ($n = 6$ per group).

technique revealed 31 microRNAs with 53 targets in $TAC_{/RIO,}$ compared to $Sham_{/RIO}$ mice (Table S5-II). Based on the mode of action of microRNAs, we next investigated whether or not up-regulated microRNAs were associated with a down-regulation of their targets resulting in reduced protein levels. We identified 'mmu-miR-21a-5p', 'mmu-miR-27b-3p', 'mmu-miR-199a-5p' and 'mmu-miR-208b-3p' to be up-regulated after TAC, which were associated with reduced protein levels mainly related to energy production and metabolism (Figure 7). The up-regulation of these microRNAs was attenuated by riociguat treatment in TAC, which coincided with attenuated down-regulation of the associated negatively correlated proteins (Figure 7 and Table S6). Correlation analyses revealed that the abundance of almost all of these microRNAs was inversely correlated with the protein levels of their putative targets (Figures 8 and S6 and Table S7).

4 | DISCUSSION

A restoration of the impaired NO-sGC-cGMP pathway is a promising new approach in the treatment of HF, as this signalling pathway controls various physiological processes, such as cardiovascular homeostasis, cellular growth and contractility (Gheorghiade et al., 2013). Interestingly, a recently published clinical trial from Armstrong et al. (2020) showed that the sGC stimulator **vericiguat** reduced the incidence of the composite of death from cardiovascular causes or hospitalisation for HF in patients with high-risk HFrEF. In experimental animals, a stimulation of the sGC has beneficial effects in HF by preventing or even reversing the progression of hypertrophy and fibrosis (Sandner, 2018). Few preclinical animal HF studies investigating the effects of riociguat on molecular changes and prolonged cardioprotective effects have been published (Pradhan et al., 2016; Rai et al., 2018). Recently, we showed that riociguat had beneficial effects on pathological cardiac remodelling, as it improved cardiac function, reversed hypertrophy, decreased fibrosis and attenuated alterations of gene expression patterns in the LV of mice exposed to TAC-induced HF (Rüdebusch et al., 2020). This is in line with our results that are presented here showing that riociguat attenuated CVD-related pathways, biological processes and functions affected by TAC up to a certain reversion in protein and microRNA expression patterns.

4.1 | Riociguat treatment attenuated and reversed TAC-induced LV proteome alterations

Progression to HF is associated with a progressive decrease in mitochondrial respiratory pathway activity (Huss & Kelly, 2005). Our previous data and our current analysis showed that energy metabolism is particularly affected by TAC (Rüdebusch et al., 2017). A large proportion of mitochondrial proteins involved in both *fatty acid β-oxidation*

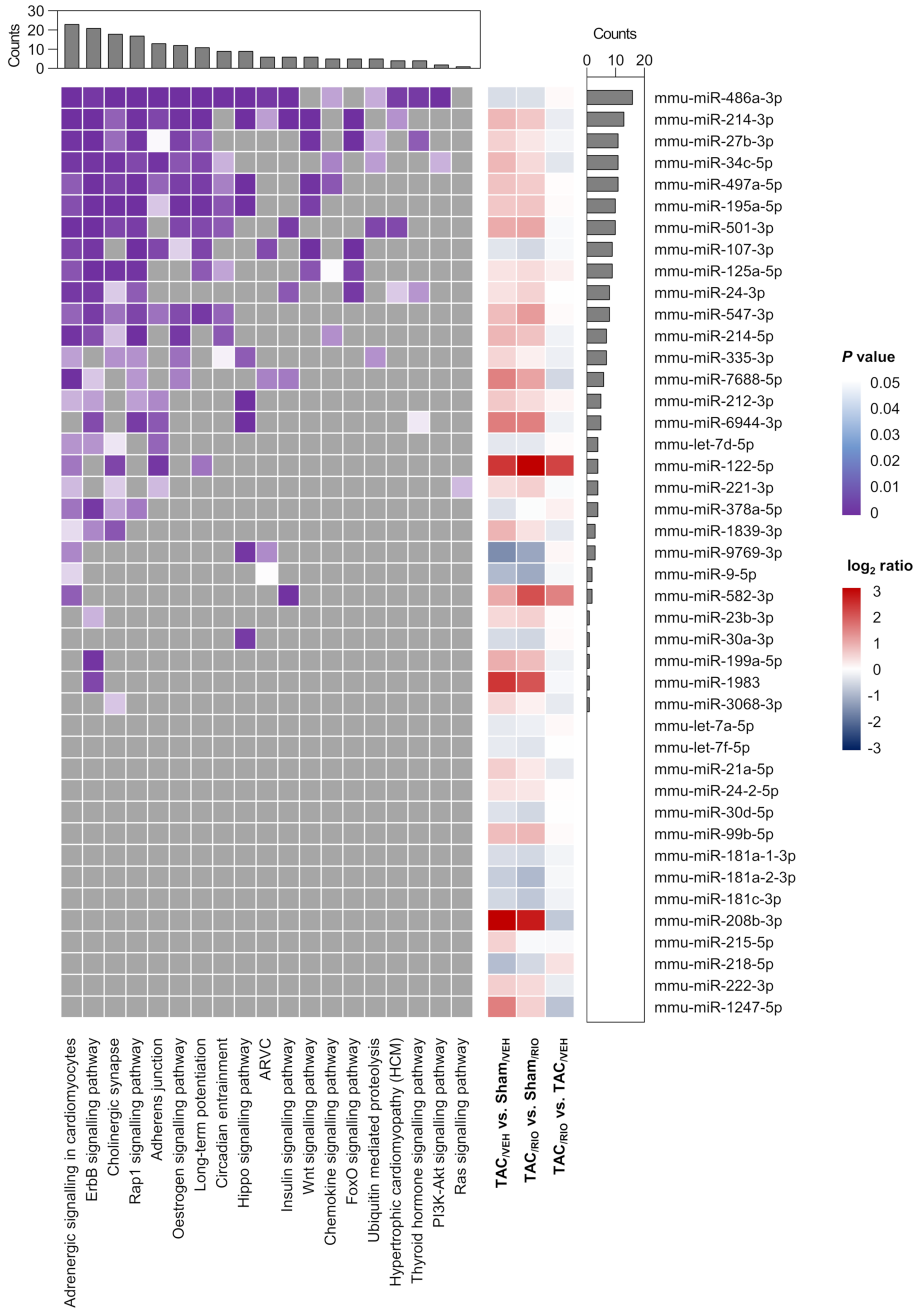

FIGURE 6 Heat maps showing the microRNA-to-pathway associations. All microRNAs with significant expression differences ($q < 0.05$) after TAC are shown together with their associations to important CVD-related pathways from miRPathDB v2.0. Functions are ordered based on their enrichment among the microRNAs (upper panel, bar chart), microRNAs based on their enrichment among functions respectively (right panel, bar chart). The right panel also shows the $\log_2$ ratios for the different comparison conditions.

and *oxidative phosphorylation* displayed reduced levels after TAC suggestive for an impaired energy supply in the LV. These results are supported by several reports from patients with HF and by data from animal studies (Bertero & Maack, 2018). Riociguat treatment reduced the total number of proteins displaying significantly altered levels. This effect became obvious in particular for mitochondrial proteins, and related metabolic pathways, functions and processes were less affected in riociguat-treated TAC mice. The global protein alterations together with functional enrichment and activation analyses results disclosed the attenuation of TAC-induced pathological cardiac processes and cardiac organ damage by riociguat administration, suggesting a beneficial influence on cardiac metabolism under HF conditions. Thus, our proteomic data further support the cardioprotective effects of riociguat treatment in HF and are in line with findings on sGC stimulation in various models of cardiac dysfunction and HF progression (Sandner, 2018). The corresponding detailed patterns of related proteins, such as the dysregulated HF markers MYH7, PLN and ANKRD1, that showed attenuation by riociguat treatment, thereby underline these findings. In small mammals, such as mice, the predominant cardiac myosin isoform during development is MYH7 and is replaced by MYH6 in the adult heart (Lompre et al., 1984). Cardiac myosin can shift to its foetal isoform in response to cardiovascular stress. This foetal gene switch, triggered by stress signalling, is relevant in disease progression (Dirkx et al., 2013). A similar cardiac-specific stress response protein and foetal gene program marker is ANKRD1, which is highly expressed in the embryonic heart, but at lower levels in the

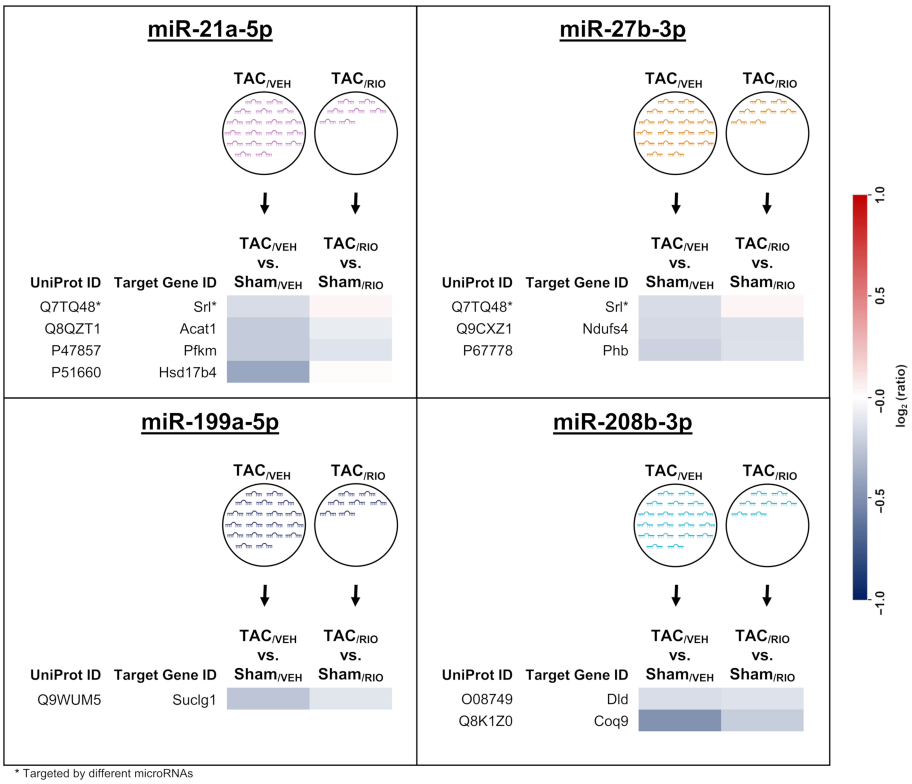

FIGURE 7 Negatively correlated microRNA–target interactions based on proteomics data. After TAC, significantly up-regulated microRNAs ($q < 0.05$) that show attenuation in expression after riociguat (RIO) treatment are displayed, together with their putative mRNA interaction partners from IPA's microRNA target filter based on the proteomics dataset. The assignment of CVD-related and heart tissue-specific targets is shown as negative correlation between up-regulation in microRNA and down-regulation in protein after TAC. Attenuated microRNA expression due to riociguat was reflected by attenuation of changes on protein level.

adult heart. ANKRD1 acts as a transcriptional regulator, as mechano-sensor and assures structural integrity of sarcomeres (Ling et al., 2017). Like MYH7, ANKRD1 was decreased in riociguat-treated TAC mice, suggesting a reversal of the foetal gene program, which underlines the beneficial and cardioprotective effects of riociguat in HF. PLN, that regulates cardiac contractility, was strongly reduced in hearts of TAC mice. Dephosphorylated PLN inhibits SERCA2a, whereas PLN phosphorylation reverses this inhibition (Kranias & Hajjar, 2012). *Pln* knockout mice exhibit a significant increase in myocardial contractility (Luo et al., 1994). The reduced PLN levels after TAC may therefore reflect a compensatory effect. Interestingly, we observed an enhanced phosphorylation of PLN (p-PLN/PLN) in TAC mice implicating an additional inhibition of PLN and de-repression of SERCA2a. Because increased PLN levels and reduced p-PLN/PLN ratios accompanied the beneficial effects of riociguat treatment in TAC mice, we hypothesise that after improvement of cardiac function this compensatory mechanism is no longer required.

4.2 | MicroRNA expression changes are involved in attenuating and reversing effects of riociguat treatment after TAC

MicroRNAs are responsible for the regulation of target gene expression and play a pivotal role in CVD. They bind to mRNA, leading to mRNA degradation or inhibition of translation (Wojciechowska et al., 2017). Several studies investigated the relation between microRNAs and their targets, using mRNA and microRNA expression data (Matkovich & Dorn, 2015; Xue et al., 2018). However, mRNA levels do not necessarily represent the exact protein levels, because translation is regulated in various different ways (Schwanhäusser et al., 2011). Nevertheless, protein profiling data and data on microRNA expression have rarely been combined, even though the alteration of microRNA expression is related to changes in the abundance of the translated protein of its target mRNA (Baek et al., 2008). Our expression and pathway analyses support the hypothesis that the identified microRNAs participate in CVD (Colpaert & Calore, 2019), and we showed that riociguat attenuated or reversed TAC-induced changes in the LV microRNA expression profiles.

Several microRNAs, such as miR-27b, miR-199a and miR-208b are known to be up-regulated in CVD (Callis et al., 2009; Pinti et al., 2017; van Rooij et al., 2009; Wang, Song, et al., 2012; Zhou et al., 2017). Among others, these three microRNAs were shown to be up-regulated after TAC and riociguat treatment had attenuated their expression in TAC animals. Overexpression of miR-27b caused left ventricular hypertrophy in mice in vivo, and its inhibition attenuated cardiac hypertrophy and dysfunction in a TAC mouse model (Wang, Song, et al., 2012). miR-199a is associated with the impairment of mitochondrial *fatty acid oxidation* in TAC enabling a metabolic shift away from the predominant reliance on fatty acids (Pinti et al., 2017). This is in line with our proteomics data indicating an impaired *β-oxidation*, further supporting the importance of microRNAs in CVD. Furthermore, miR-208b and MYH7 showed the highest alteration in abundance due to TAC. Interestingly, the TAC-mediated increase of miR-208b and MYH7 was strongly attenuated by riociguat indicative of mutual co-regulation of both. Importantly, miR-208b is encoded

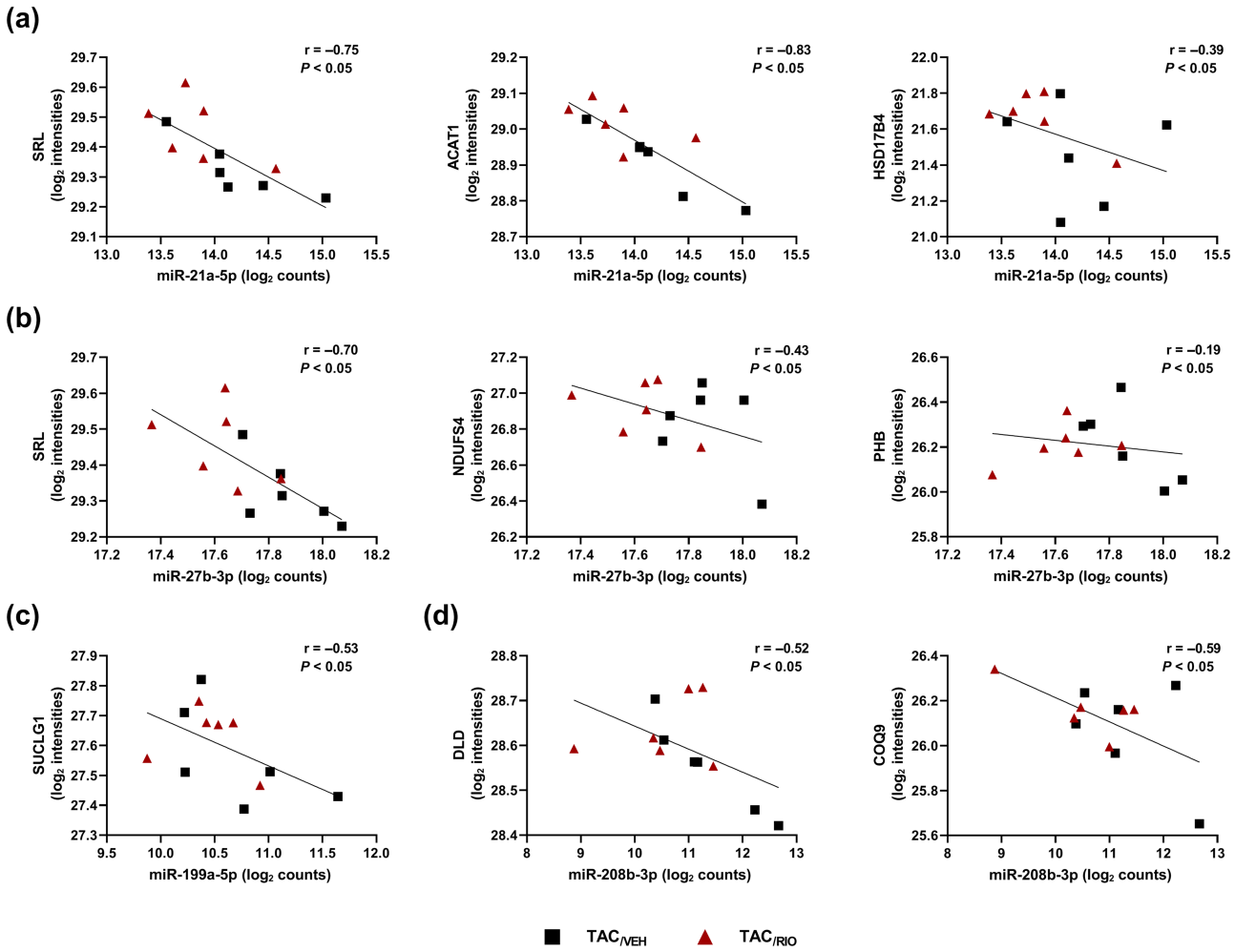

FIGURE 8 Correlation analyses between microRNA and protein levels from IPA's predicted microRNA–target interactions based on proteomics data. Pearson correlations between log_2-transformed values of microRNA-Seq counts and protein intensities from MS are presented as scatter plots for single samples of $TAC_{/VEH}$ together with $TAC_{/RIO}$. The line drawn in every graph is for visualisation of direction. The displayed levels of microRNAs in $TAC_{/VEH}$ and $TAC_{/RIO}$ were all inversely correlated with the protein intensities of their putative mRNA targets. (a) miR-21a-5p. (b) miR-27b-3p. (c) miR-199a-5p. (d) miR-208b-3p. Detailed information on correlation and significance for the individual groups are provided in Figure S6 and Table S7 (ACAT1, acetyl-CoA acetyltransferase; COQ9, ubiquinone biosynthesis protein COQ9; DLD, dihydrolipoyl dehydrogenase; HSD17B4, peroxisomal multifunctional enzyme type 2; NDUFS4, NADH dehydrogenase [ubiquinone] iron–sulphur protein 4; PHB, prohibitin; SRL, sarcalumenin; SUCLG1, succinyl-CoA ligase [ADP/GDP-forming] subunit alpha).

within the *Myh7* gene and thereby parallels its host gene expression (Callis et al., 2009). As part of the so-called MyomiR regulatory network of microRNAs located within and coexpressed with their corresponding myosin genes, *Myh7/miR-208b* are only expressed upon stress and thus appear to adapt cardiac gene expression to physiological and pathological signalling (van Rooij et al., 2009). Moreover, Zhou et al. (2017) showed that the inhibition of miR-208b in a mouse model of dilated cardiomyopathy prevented the transition of adaptive to maladaptive cardiac remodelling and improved cardiac function. miR-208b also targets the repressors of *Myh7* thereby promoting the expression of *Myh7* itself and contributing to the continuance of the foetal gene switch (van Rooij et al., 2009). Another link exists between ANKRD1 and miR-199a, which targets the *Ankrd1* transcript. As discussed before, the abundance of ANKRD1 was increased in TAC mice, which is in contrast to the increased miR-199a expression. Thus, up-regulation of miR-199a might be part of a compensatory response to counteract ANKRD1 induction in hypertrophic hearts (Ling et al., 2017).

PLN seems to have an unusual microRNA antagonist. miR-21a was highly up-regulated in $TAC_{/VEH}$, but not in $TAC_{/RIO}$ hearts. Of note, miR-21a contributes to the inhibition of PLN via an off-target effect. Soller et al. (2016) showed that miR-21 (previous ID of miR-21a) inhibits PLN by directly binding to it. For some of the identified microRNAs with the strongest changes in expression like 'mmu-miR-7688-5p', 'mmu-miR-6944-3p' and 'mmu-miR-9769-3p' almost nothing is known. These microRNAs have only very recently been discovered (Ambros et al., 2003). Due to their strong alteration by TAC and their attenuation by riociguat treatment, they seem to be important for CVD. However, further analyses are needed to support this idea. Riociguat treatment also intensified expression of specific

microRNAs, such as miR-24 and miR-122, after TAC. These microRNAs have shown anti-fibrotic properties in different rodent models, suggesting an effect of riociguat on microRNA-related fibrotic remodelling (Sun et al., 2018; Wang, Huang, et al., 2012). In addition, these FibromiRs in general hold promise for the development of anti-fibrotic drugs (Pottier et al., 2014).

4.3 | Comparison of therapeutic effects of riociguat with other cGMP augmenting therapies

In cardiovascular tissue, two enzymes are important for generating cGMP: the membrane-bound **guanylyl cyclase**, which is activated by natriuretic peptides (NP), and the sGC activated by NO (Richards et al., 2021). As a therapeutic target, cGMP received much attention in both basic and clinical research on HF treatment, as it transmits NO- and NP-coupled signalling and has cardioprotective effects (Blanton, 2020; Friebe et al., 2020). An increase in cGMP can be achieved by enhanced cGMP synthesis or inhibition of its degradation by phosphodiesterases (PDEs). However, an increase in cGMP levels may be counteracted by an increased PDE activity (Lee et al., 2015). Recently, we showed that direct sGC stimulation by riociguat treatment that increases cGMP synthesis had beneficial effects in a HF mouse model (Rüdebusch et al., 2020). In addition, several cGMP-elevating therapies have proven their cardioprotective potential, as discussed in our previous study (Rüdebusch et al., 2020). For example, anti-fibrotic and anti-hypertrophic effects prevent cardiac remodelling with deactivation or even reversal of multiple hypertrophy and fibrosis signalling pathways. This was accompanied by an improved cardiac function and demonstrated in various models of hypertrophy and HF in vivo and in vitro (Burke et al., 2019; Lee et al., 2015; Richards et al., 2021; Zhang et al., 2010). Similar effects were also reported for sGC activators. Several studies have shown that modulating the NO-sGC-cGMP pathway has cardioprotective effects, either by pharmacological NO-GC modulators or by inhibitors of cGMP degrading PDEs (Blanton, 2020). Recently, Mishra et al. showed that cGMP-selective **PDE 9A** inhibition (PDE9-I) stimulates mitochondrial activity and improves cardiometabolic syndrome in a mouse model of diet-induced obesity after mild TAC in vivo. Such inhibition of PDE 9A reduced hypertrophy, fibrosis and corresponding molecular signalling. Further, this work also showed that inhibition of PDE 9A increased mitochondrial respiration and fatty acid oxidation also in cardiomyocytes in vitro (Mishra et al., 2021). These findings are in line with our results of improved metabolism and energy production after riociguat treatment in TAC, which further supports the evidence of beneficial effects from different strategies of cGMP augmentation in different settings of CVD. In this context, CRD-733, acting as a novel inhibitor of the cGMP-degrading PDE9, also reversed LV hypertrophy, attenuated gene expression of HF markers and improved LV function in a mouse model of pressure overload-induced HF (Richards et al., 2021). To the best of our knowledge, there is no comparable study that has conducted detailed global proteome or microRNA analyses in the way we did. Current clinical and experimental data provide evidence that cGMP-generating compounds have beneficial effects in HF and our present work thus clearly expands the existing knowledge on cGMP-enhancing therapies.

The beneficial effects of sGC stimulators, such as riociguat and also other cGMP augmenting therapies in CVD may be mediated by an activation of **protein kinase G1 (PKG1)** (Adler et al., 2020; Blanton, 2020). Both cGMP and its main effector kinase PKG1 generally counteract molecular aberrations that contribute to HF (Blanton, 2020). cGMP-PKG1 signalling is involved in the Ca^{2+} handling in cardiomyocytes and regulates the influx of Ca^{2+} by interfering with sarcomeric proteins and proteins located at the SR, such as by phosphorylation of PLN at the serine residue at position 16 (Ser16) (Adler et al., 2020). In line with these findings, we also observed an increased Ser16 phosphorylation of PLN after riociguat treatment in TAC, even though the p-PLN/PLN ratio seemed to be slightly reversed, compared to untreated TAC mice. However, we did not observe an increased PLN phosphorylation in $Sham_{/RIO}$ animals, suggesting that compensatory mechanisms counteract elevations in cGMP in healthy animals. Interestingly, the protein levels of total PLN were significantly decreased in mice with cardiomyocyte-restricted deletion of *Prkg1* (encoding PKG1) in response to TAC, when compared to wild-type littermate controls (Frantz et al., 2013). In addition, the **PDE5** inhibitor **sildenafil** improved the cGMP-PKG1 activity, which was accompanied by an increased PLN gene expression and protein abundance, improved calcium handling and attenuated molecular remodelling in TAC-induced HF in mice (Nagayama et al., 2009). This suggests that both the increased PLN phosphorylation and the increased levels of total PLN after riociguat treatment in TAC mice are PKG1-dependent. However, a recent in vivo study with genetically modified mice with constitutive, cGMP-independent PKG1 activation showed that long-term activation of PKG1 could even be detrimental to the heart, especially after pressure overload or neurohumoral stress (Schwaerzer et al., 2021). As clinical trials of cGMP-elevating agents have yielded mixed results, this may explain some of the controversial data (Blanton, 2020; Schwaerzer et al., 2021). Although the discussed presumptions suggest a PKG1 dependency, PKG1-independent effects may need to be considered, as well, and require further investigation.

Based on the marked effects of riociguat on cardiac structure and function in our HF mouse model, we expected many and very marked molecular differences between TAC animals treated with riociguat, compared to those treated with VEH. However, the molecular alterations detected were rather moderate. Nevertheless, riociguat treatment did attenuate TAC-induced alterations of LV protein and microRNA patterns and associated functional perturbations during chronic pressure overload-induced HF. Our work shows that the sGC stimulator riociguat has beneficial effects on pathological cardiac remodelling. The results also imply that relatively small corrections in the LV proteome and microRNAs by riociguat can have major consequences for cardiac function in TAC-induced HF.

ACKNOWLEDGEMENTS

We would like to thank Dr. Eric Witt for his assistance and guidance in the integrative, statistical analysis of large-scale proteomics data

using Genedata® Analyst™ software. Further, we would like to acknowledge BioRender.com that was used to create parts of the figures.

This work was supported by the German Centre for Cardiovascular Research (DZHK, Deutsches Zentrum für Herz-Kreislaufforschung), partner site Greifswald (Grant DZHK 81Z5400153 to S.B.F. and J.F.). L.K. acknowledges funding from the European Union H2020 Programme (euCanSHare) (Grant 825903). Open Access funding enabled and organized by Projekt DEAL.

CONFLICT OF INTEREST

Dr. Felix has received consulting fees and speaker honoraria by Bayer Health Care (minor). The remaining authors have disclosed that they do not have any conflicts of interest.

AUTHOR CONTRIBUTIONS

A.B., J.F., J.R., K.G. and S.B.F conceived and designed the research. A.B. designed, performed and analysed experiments, discussed data and wrote the manuscript. A.B., E.H., J.F., J.R., K.G., S.G. and S.B.F. interpreted results of experiments. A.B. and N.N. prepared figures. E.H., J.F., J.R., N. N, S.B.F. and U.V. edited and revised the manuscript. A.B., E.H., G.E., J.F., J.R., K.G., L.K., N.N., S.B.F., S.G., T.M., U.V. and V.M.D. approved final version of manuscript. J.R. conducted animal surgery. V.M.D. performed mass spectrometric measurements. E.H. and U.V. supervised mass spectrometric measurements and analysis. G.E. and T.M. performed microRNA sequencing. N.N. performed bioinformatics analyses for microRNA sequencing data. All authors declare that the submitted work has not been published before (neither in English nor in any other language) and that the work is not under consideration for publication elsewhere.

DECLARATION OF TRANSPARENCY AND SCIENTIFIC RIGOUR

This Declaration acknowledges that this paper adheres to the principles for transparent reporting and scientific rigour of preclinical research as stated in the BJP guidelines for Design & Analysis, Immunoblotting and Immunochemistry and Animal Experimentation, and as recommended by funding agencies, publishers and other organisations engaged with supporting research.

DATA AVAILABILITY STATEMENT

The mass spectrometry proteomics data have been deposited with the ProteomeXchange Consortium via the PRIDE (Perez-Riverol et al., 2019) partner repository with the dataset identifier PXD024156. All microRNA-Seq fastq data are available at the Sequence Read Archive (BioSample accession SAMN17674846 and BioProject: PRJNA697862).

ORCID

Alexander Benkner https://orcid.org/0000-0002-3415-0512

REFERENCES

Adler, J., Kuret, A., Längst, N., & Lukowski, R. (2020). Targets of cGMP/cGKI in cardiac myocytes. *Journal of Cardiovascular Pharmacology*, *75*(6), 494–507. https://doi.org/10.1097/fjc.0000000000000817

Alexander, S. P. H., Fabbro, D., Kelly, E., Mathie, A., Peters, J. A., Veale, E. L., Armstrong, J. F., Faccenda, E., Harding, S. D., Pawson, A. J., Southan, C., Davies, J. A., Beuve, A., Brouckaert, P., Bryant, C., Burnett, J. C., Farndale, R. W., Friebe, A., Garthwaite, J., … Waldman, S. A. (2021). THE CONCISE GUIDE TO PHARMACOLOGY 2021/22: Catalytic receptors. *British Journal of Pharmacology*, *178*, S264–S312. https://doi.org/10.1111/bph.15541

Alexander, S. P. H., Fabbro, D., Kelly, E., Mathie, A., Peters, J. A., Veale, E. L., Armstrong, J. F., Faccenda, E., Harding, S. D., Pawson, A. J., Southan, C., Davies, J. A., Boison, D., Burns, K. E., Dessauer, C., Gertsch, J., Helsby, N. A., Izzo, A. A., Koesling, D., … Wong, S. S. (2021). THE CONCISE GUIDE TO PHARMACOLOGY 2021/22: Enzymes. *British Journal of Pharmacology*, *178*(S1), S313–S411. https://doi.org/10.1111/bph.15542

Ambros, V., Bartel, B., Bartel, D. P., Burge, C. B., Carrington, J. C., Chen, X., Dreyfuss, G., Eddy, S. R., Griffiths-Jones, S., Marshall, M., Matzke, M., Ruvkun, G., & Tuschl, T. (2003). A uniform system for microRNA annotation. *RNA*, *9*(3), 277–279. https://doi.org/10.1261/rna.2183803

An, J., Lai, J., Lehman, M. L., & Nelson, C. C. (2013). miRDeep*: An integrated application tool for miRNA identification from RNA sequencing data. *Nucleic Acids Research*, *41*(2), 727–737. https://doi.org/10.1093/nar/gks1187

Armstrong, P. W., Pieske, B., Anstrom, K. J., Ezekowitz, J., Hernandez, A. F., Butler, J., Lam, C. S. P., Ponikowski, P., Voors, A. A., Jia, G., McNulty, S. E., Patel, M. J., Roessig, L., Koglin, J., & O'Connor, C. M. (2020). Vericiguat in patients with heart failure and reduced ejection fraction. *The New England Journal of Medicine*, *382*(20), 1883–1893. https://doi.org/10.1056/NEJMoa1915928

Baek, D., Villén, J., Shin, C., Camargo, F. D., Gygi, S. P., & Bartel, D. P. (2008). The impact of microRNAs on protein output. *Nature*, *455*(7209), 64–71. https://doi.org/10.1038/nature07242

Bernardo, B. C., Weeks, K. L., Pretorius, L., & McMullen, J. R. (2010). Molecular distinction between physiological and pathological cardiac hypertrophy: Experimental findings and therapeutic strategies. *Pharmacology & Therapeutics*, *128*(1), 191–227. https://doi.org/10.1016/j.pharmthera.2010.04.005

Bertero, E., & Maack, C. (2018). Metabolic remodelling in heart failure. *Nature Reviews. Cardiology*, *15*(8), 457–470. https://doi.org/10.1038/s41569-018-0044-6

Blanton, R. M. (2020). cGMP signaling and modulation in heart failure. *Journal of Cardiovascular Pharmacology*, *75*(5), 385–398. https://doi.org/10.1097/fjc.0000000000000749

Bonnet, E., Wuyts, J., Rouzé, P., & Van de Peer, Y. (2004). Evidence that microRNA precursors, unlike other non-coding RNAs, have lower folding free energies than random sequences. *Bioinformatics*, *20*(17), 2911–2917. https://doi.org/10.1093/bioinformatics/bth374

Burke, R. M., Lighthouse, J. K., Mickelsen, D. M., & Small, E. M. (2019). Sacubitril/valsartan decreases cardiac fibrosis in left ventricle pressure overload by restoring PKG signaling in cardiac fibroblasts. *Circulation. Heart Failure*, *12*(4), e005565. https://doi.org/10.1161/circheartfailure.118.005565

Callis, T. E., Pandya, K., Seok, H. Y., Tang, R. H., Tatsuguchi, M., Huang, Z. P., Chen, J. F., Deng, Z., Gunn, B., Shumate, J., Willis, M. S., Selzman, C. H., & Wang, D. Z. (2009). MicroRNA-208a is a regulator of cardiac hypertrophy and conduction in mice. *The Journal of Clinical Investigation*, *119*(9), 2772–2786. https://doi.org/10.1172/jci36154

Chen, Z., Liu, J., Ng, H. K., Nadarajah, S., Kaufman, H. L., Yang, J. Y., & Deng, Y. (2011). Statistical methods on detecting differentially expressed genes for RNA-seq data. *BMC Systems Biology*, *5*(Suppl 3), S1. https://doi.org/10.1186/1752-0509-5-s3-s1

Colpaert, R. M. W., & Calore, M. (2019). MicroRNAs in cardiac diseases. *Cell*, *8*(7). https://doi.org/10.3390/cells8070737

Cox, J., Hein, M. Y., Luber, C. A., Paron, I., Nagaraj, N., & Mann, M. (2014). Accurate proteome-wide label-free quantification by delayed normalization and maximal peptide ratio extraction, termed MaxLFQ. *Molecular & Cellular Proteomics*, *13*(9), 2513–2526. https://doi.org/10.1074/mcp.M113.031591

Curtis, M. J., Alexander, S., Cirino, G., Docherty, J. R., George, C. H., Giembycz, M. A., Hoyer, D., Insel, P. A., Izzo, A. A., Ji, Y., MacEwan, D. J., Sobey, C. G., Stanford, S. C., Teixeira, M. M., Wonnacott, S., & Ahluwalia, A. (2018). Experimental design and analysis and their reporting II: Updated and simplified guidance for authors and peer reviewers. *British Journal of Pharmacology*, *175*(7), 987–993. https://doi.org/10.1111/bph.14153

Dirkx, E., da Costa Martins, P. A., & De Windt, L. J. (2013). Regulation of fetal gene expression in heart failure. *Biochimica et Biophysica Acta*, *1832*(12), 2414–2424. https://doi.org/10.1016/j.bbadis.2013.07.023

Frantz, S., Klaiber, M., Baba, H. A., Oberwinkler, H., Völker, K., Gaβner, B., Bayer, B., Abeβer, M., Schuh, K., Feil, R., Hofmann, F., & Kuhn, M. (2013). Stress-dependent dilated cardiomyopathy in mice with cardiomyocyte-restricted inactivation of cyclic GMP-dependent protein kinase I. *European Heart Journal*, *34*(16), 1233–1244. https://doi.org/10.1093/eurheartj/ehr445

Friebe, A., Sandner, P., & Schmidtko, A. (2020). cGMP: A unique 2nd messenger molecule—Recent developments in cGMP research and development. *Naunyn-Schmiedeberg's Archives of Pharmacology*, *393*(2), 287–302. https://doi.org/10.1007/s00210-019-01779-z

Gheorghiade, M., Marti, C. N., Sabbah, H. N., Roessig, L., Greene, S. J., Böhm, M., Burnett, J. C., Campia, U., Cleland, J. G., Collins, S. P., Fonarow, G. C., Levy, P. D., Metra, M., Pitt, B., Ponikowski, P., Sato, N., Voors, A. A., Stasch, J. P., Butler, J., & Academic Research Team in Heart Failure (ART-HF). (2013). Soluble guanylate cyclase: A potential therapeutic target for heart failure. *Heart Failure Reviews*, *18*(2), 123–134. https://doi.org/10.1007/s10741-012-9323-1

Gürtler, A., Kunz, N., Gomolka, M., Hornhardt, S., Friedl, A. A., McDonald, K., Kohn, J. E., & Posch, A. (2013). Stain-free technology as a normalization tool in Western blot analysis. *Analytical Biochemistry*, *433*(2), 105–111. https://doi.org/10.1016/j.ab.2012.10.010

Huss, J. M., & Kelly, D. P. (2005). Mitochondrial energy metabolism in heart failure: A question of balance. *The Journal of Clinical Investigation*, *115*(3), 547–555. https://doi.org/10.1172/jci24405

Kehl, T., Kern, F., Backes, C., Fehlmann, T., Stöckel, D., Meese, E., Lenhof, H. P., & Keller, A. (2020). miRPathDB 2.0: A novel release of the miRNA Pathway Dictionary Database. *Nucleic Acids Research*, *48*(D1), D142–D147. https://doi.org/10.1093/nar/gkz1022

Kramer, A., Green, J., Pollard, J. Jr., & Tugendreich, S. (2014). Causal analysis approaches in ingenuity pathway analysis. *Bioinformatics*, *30*(4), 523–530. https://doi.org/10.1093/bioinformatics/btt703

Kranias, E. G., & Hajjar, R. J. (2012). Modulation of cardiac contractility by the phospholamban/SERCA2a regulatome. *Circulation Research*, *110*(12), 1646–1660. https://doi.org/10.1161/circresaha.111.259754

Lee, D. I., Zhu, G., Sasaki, T., Cho, G.-S., Hamdani, N., Holewinski, R., Jo, S. H., Danner, T., Zhang, M., Rainer, P. P., Bedja, D., Kirk, J. A., Ranek, M. J., Dostmann, W. R., Kwon, C., Margulies, K. B., van Eyk, J. E., Paulus, W. J., Takimoto, E., & Kass, D. A. (2015). Phosphodiesterase 9A controls nitric-oxide-independent cGMP and hypertrophic heart disease. *Nature*, *519*(7544), 472–476. https://doi.org/10.1038/nature14332

Lilley, E., Stanford, S. C., Kendall, D. E., Alexander, S. P. H., Cirino, G., Docherty, J. R., George, C. H., Insel, P. A., Izzo, A. A., Ji, Y., Panettieri, R. A., Sobey, C. G., Stefanska, B., Stephens, G., Teixeira, M., & Ahluwalia, A. (2020). ARRIVE 2.0 and the British Journal of Pharmacology: Updated guidance for 2020. *British Journal of Pharmacology*, *177*(16), 3611–3616. https://doi.org/10.1111/bph.15178

Linden, K., Mailey, J., Kearney, A., & Menown, I. B. A. (2020). Advances in clinical cardiology 2019: A summary of key clinical trials. *Advances in Therapy*, *37*(6), 2620–2645. https://doi.org/10.1007/s12325-020-01355-5

Ling, S. S. M., Chen, Y. T., Wang, J., Richards, A. M., & Liew, O. W. (2017). Ankyrin repeat domain 1 protein: A functionally pleiotropic protein with cardiac biomarker potential. *International Journal of Molecular Sciences*, *18*(7), 1362. https://doi.org/10.3390/ijms18071362

Livak, K. J., & Schmittgen, T. D. (2001). Analysis of relative gene expression data using real-time quantitative PCR and the $2^{-\Delta\Delta CT}$ method. *Methods*, *25*(4), 402–408. https://doi.org/10.1006/meth.2001.1262

Lompre, A. M., Nadal-Ginard, B., & Mahdavi, V. (1984). Expression of the cardiac ventricular alpha- and beta-myosin heavy chain genes is developmentally and hormonally regulated. *The Journal of Biological Chemistry*, *259*(10), 6437–6446. https://doi.org/10.1016/S0021-9258(20)82162-0

Love, M. I., Huber, W., & Anders, S. (2014). Moderated estimation of fold change and dispersion for RNA-seq data with DESeq2. *Genome Biology*, *15*(12), 550. https://doi.org/10.1186/s13059-014-0550-8

Luo, W., Grupp, I. L., Harrer, J., Ponniah, S., Grupp, G., Duffy, J. J., Doetschman, T., & Kranias, E. G. (1994). Targeted ablation of the phospholamban gene is associated with markedly enhanced myocardial contractility and loss of beta-agonist stimulation. *Circulation Research*, *75*(3), 401–409. https://doi.org/10.1161/01.res.75.3.401

Matkovich, S. J., & Dorn, G. W. II (2015). Deep sequencing of cardiac microRNA-mRNA interactomes in clinical and experimental cardiomyopathy. *Methods in Molecular Biology*, *1299*, 27–49. https://doi.org/10.1007/978-1-4939-2572-8_3

Mishra, S., Sadagopan, N., Dunkerly-Eyring, B., Rodriguez, S., Sarver, D. C., Ceddia, R. P., & Kass, D. A. (2021). Inhibition of phosphodiesterase type 9 reduces obesity and cardiometabolic syndrome in mice. *The Journal of Clinical Investigation*, *131*(21), e148798. https://doi.org/10.1172/jci148798

Mitrovic, V., Jovanovic, A., & Lehinant, S. (2011). Soluble guanylate cyclase modulators in heart failure. *Current Heart Failure Reports*, *8*(1), 38–44. https://doi.org/10.1007/s11897-010-0045-1

Mittendorf, J., Weigand, S., Alonso-Alija, C., Bischoff, E., Feurer, A., Gerisch, M., Kern, A., Knorr, A., Lang, D., Muenter, K., Radtke, M., Schirok, H., Schlemmer, K. H., Stahl, E., Straub, A., Wunder, F., & Stasch, J. P. (2009). Discovery of riociguat (BAY 63-2521): A potent, oral stimulator of soluble guanylate cyclase for the treatment of pulmonary hypertension. *ChemMedChem*, *4*(5), 853–865. https://doi.org/10.1002/cmdc.200900014

Murphy, S. P., Ibrahim, N. E., & Januzzi, J. L. Jr. (2020). Heart failure with reduced ejection fraction: A review. *JAMA*, *324*(5), 488–504. https://doi.org/10.1001/jama.2020.10262

Nagayama, T., Hsu, S., Zhang, M., Koitabashi, N., Bedja, D., Gabrielson, K. L., Takimoto, E., & Kass, D. A. (2009). Sildenafil stops progressive chamber, cellular, and molecular remodeling and improves calcium handling and function in hearts with pre-existing advanced hypertrophy caused by pressure overload. *Journal of the American College of Cardiology*, *53*(2), 207–215. https://doi.org/10.1016/j.jacc.2008.08.069

Percie du Sert, N., Hurst, V., Ahluwalia, A., Alam, S., Avey, M. T., Baker, M., Browne, W. J., Clark, A., Cuthill, I. C., Dirnagl, U., Emerson, M., Garner, P., Holgate, S. T., Howells, D. W., Karp, N. A., Lazic, S. E., Lidster, K., MacCallum, C. J., Macleod, M., … Würbel, H. (2020). The ARRIVE guidelines 2.0: Updated guidelines for reporting animal research. *British Journal of Pharmacology*, *177*(16), 3617–3624. https://doi.org/10.1111/bph.15193

Perez-Riverol, Y., Csordas, A., Bai, J., Bernal-Llinares, M., Hewapathirana, S., Kundu, D. J., Inuganti, A., Griss, J., Mayer, G.,

Eisenacher, M., Pérez, E., Uszkoreit, J., Pfeuffer, J., Sachsenberg, T., Yılmaz, Ş., Tiwary, S., Cox, J., Audain, E., Walzer, M., … Vizcaíno, J. A. (2019). The PRIDE database and related tools and resources in 2019: Improving support for quantification data. *Nucleic Acids Research*, *47*(D1), D442–D450. https://doi.org/10.1093/nar/gky1106

Pinti, M. V., Hathaway, Q. A., & Hollander, J. M. (2017). Role of microRNA in metabolic shift during heart failure. *American Journal of Physiology. Heart and Circulatory Physiology*, *312*(1), H33–h45. https://doi.org/10.1152/ajpheart.00341.2016

Ponikowski, P., Voors, A. A., Anker, S. D., Bueno, H., Cleland, J. G. F., Coats, A. J. S., Falk, V., González-Juanatey, J. R., Harjola, V. P., Jankowska, E. A., Jessup, M., Linde, C., Nihoyannopoulos, P., Parissis, J. T., Pieske, B., Riley, J. P., Rosano, G. M. C., Ruilope, L. M., Ruschitzka, F., … ESC Scientific Document Group. (2016). 2016 ESC Guidelines for the diagnosis and treatment of acute and chronic heart failure: The Task Force for the diagnosis and treatment of acute and chronic heart failure of the European Society of Cardiology (ESC) developed with the special contribution of the Heart Failure Association (HFA) of the ESC. *European Heart Journal*, *37*(27), 2129–2200. https://doi.org/10.1093/eurheartj/ehw128

Pottier, N., Cauffiez, C., Perrais, M., Barbry, P., & Mari, B. (2014). FibromiRs: Translating molecular discoveries into new anti-fibrotic drugs. *Trends in Pharmacological Sciences*, *35*(3), 119–126. https://doi.org/10.1016/j.tips.2014.01.003

Pradhan, K., Sydykov, A., Tian, X., Mamazhakypov, A., Neupane, B., Luitel, H., Weissmann, N., Seeger, W., Grimminger, F., Kretschmer, A., Stasch, J. P., Ghofrani, H. A., & Schermuly, R. T. (2016). Soluble guanylate cyclase stimulator riociguat and phosphodiesterase 5 inhibitor sildenafil ameliorate pulmonary hypertension due to left heart disease in mice. *International Journal of Cardiology*, *216*, 85–91. https://doi.org/10.1016/j.ijcard.2016.04.098

Rai, N., Veeroju, S., Schymura, Y., Janssen, W., Wietelmann, A., Kojonazarov, B., Weissmann, N., Stasch, J. P., Ghofrani, H. A., Seeger, W., Schermuly, R. T., & Novoyatleva, T. (2018). Effect of riociguat and sildenafil on right heart remodeling and function in pressure overload induced model of pulmonary arterial banding. *BioMed Research International*, *2018*, 3293584. https://doi.org/10.1155/2018/3293584

Richards, D. A., Aronovitz, M. J., Liu, P., Martin, G. L., Tam, K., Pande, S., Karas, R. H., Bloomfield, D. M., Mendelsohn, M. E., & Blanton, R. M. (2021). CRD-733, a novel PDE9 (phosphodiesterase 9) inhibitor, reverses pressure overload–induced heart failure. *Circulation. Heart Failure*, *14*(1), e007300. https://doi.org/10.1161/CIRCHEARTFAILURE.120.007300

Rüdebusch, J., Benkner, A., Nath, N., Fleuch, L., Kaderali, L., Grube, K., Klingel, K., Eckstein, G., Meitinger, T., Fielitz, J., & Felix, S. B. (2020). Stimulation of soluble guanylyl cyclase (sGC) by riociguat attenuates heart failure and pathological cardiac remodelling. *British Journal of Pharmacology*, *179*, 2430–2442. https://doi.org/10.1111/bph.15333

Rüdebusch, J., Benkner, A., Poesch, A., Dörr, M., Völker, U., Grube, K., Hammer, E., & Felix, S. B. (2017). Dynamic adaptation of myocardial proteome during heart failure development. *PLoS ONE*, *12*(10), e0185915. https://doi.org/10.1371/journal.pone.0185915

Sandner, P. (2018). From molecules to patients: Exploring the therapeutic role of soluble guanylate cyclase stimulators. *Biological Chemistry*, *399*(7), 679–690. https://doi.org/10.1515/hsz-2018-0155

Schwaerzer, G. K., Casteel, D. E., Cividini, F., Kalyanaraman, H., Zhuang, S., Gu, Y., Dalton, N. D., Peterson, K. L., Dillmann, W. H., Boss, G. R., & Pilz, R. B. (2021). Constitutive protein kinase G activation exacerbates stress-induced cardiomyopathy. *British Journal of Pharmacology*, *179*, 2413–2429. https://doi.org/10.1111/bph.15530

Schwanhäusser, B., Busse, D., Li, N., Dittmar, G., Schuchhardt, J., Wolf, J., Chen, W., & Selbach, M. (2011). Global quantification of mammalian gene expression control. *Nature*, *473*(7347), 337–342. https://doi.org/10.1038/nature10098

Shah, R. C., Sanker, S., Wood, K. C., Durgin, B. G., & Straub, A. C. (2018). Redox regulation of soluble guanylyl cyclase. *Nitric Oxide*, *76*, 97–104. https://doi.org/10.1016/j.niox.2018.03.013

Soller, K. J., Yang, J., Veglia, G., & Bowser, M. T. (2016). Reversal of phospholamban inhibition of the sarco(endo)plasmic reticulum Ca^{2+}-ATPase (SERCA) using short, protein-interacting RNAs and oligonucleotide analogs. *The Journal of Biological Chemistry*, *291*(41), 21510–21518. https://doi.org/10.1074/jbc.M116.738807

Stasch, J. P., & Hobbs, A. J. (2009). NO-independent, haem-dependent soluble guanylate cyclase stimulators. *Handbook of Experimental Pharmacology*, (191), 277–308. https://doi.org/10.1007/978-3-540-68964-5_13

Stasch, J. P., Pacher, P., & Evgenov, O. V. (2011). Soluble guanylate cyclase as an emerging therapeutic target in cardiopulmonary disease. *Circulation*, *123*(20), 2263–2273. https://doi.org/10.1161/circulationaha.110.981738

Stöckel, D., Kehl, T., Trampert, P., Schneider, L., Backes, C., Ludwig, N., Gerasch, A., Kaufmann, M., Gessler, M., Graf, N., Meese, E., Keller, A., & Lenhof, H. P. (2016). Multi-omics enrichment analysis using the GeneTrail2 web service. *Bioinformatics*, *32*(10), 1502–1508. https://doi.org/10.1093/bioinformatics/btv770

Sun, Y., Wang, H., Li, Y., Liu, S., Chen, J., & Ying, H. (2018). miR-24 and miR-122 negatively regulate the transforming growth factor-β/Smad signaling pathway in skeletal muscle fibrosis. *Molecular Therapy - Nucleic Acids*, *11*, 528–537. https://doi.org/10.1016/j.omtn.2018.04.005

Umar, S., & van der Laarse, A. (2010). Nitric oxide and nitric oxide synthase isoforms in the normal, hypertrophic, and failing heart. *Molecular and Cellular Biochemistry*, *333*(1–2), 191–201. https://doi.org/10.1007/s11010-009-0219-x

van Rooij, E., Quiat, D., Johnson, B. A., Sutherland, L. B., Qi, X., Richardson, J. A., Kelm, R. J. Jr., & Olson, E. N. (2009). A family of microRNAs encoded by myosin genes governs myosin expression and muscle performance. *Developmental Cell*, *17*(5), 662–673. https://doi.org/10.1016/j.devcel.2009.10.013

Wang, J., Huang, W., Xu, R., Nie, Y., Cao, X., Meng, J., Xu, X., Hu, S., & Zheng, Z. (2012). MicroRNA-24 regulates cardiac fibrosis after myocardial infarction. *Journal of Cellular and Molecular Medicine*, *16*(9), 2150–2160. https://doi.org/10.1111/j.1582-4934.2012.01523.x

Wang, J., Song, Y., Zhang, Y., Xiao, H., Sun, Q., Hou, N., Guo, S., Wang, Y., Fan, K., Zhan, D., Zha, L., Cao, Y., Li, Z., Cheng, X., Zhang, Y., & Yang, X. (2012). Cardiomyocyte overexpression of miR-27b induces cardiac hypertrophy and dysfunction in mice. *Cell Research*, *22*(3), 516–527. https://doi.org/10.1038/cr.2011.132

Wojciechowska, A., Braniewska, A., & Kozar-Kamińska, K. (2017). MicroRNA in cardiovascular biology and disease. *Advances in Clinical and Experimental Medicine*, *26*(5), 865–874. https://doi.org/10.17219/acem/62915

Xue, J., Zhou, D., Poulsen, O., Hartley, I., Imamura, T., Xie, E. X., & Haddad, G. G. (2018). Exploring miRNA-mRNA regulatory network in cardiac pathology in Na^{+}/H^{+} exchanger isoform 1 transgenic mice. *Physiological Genomics*, *50*(10), 846–861. https://doi.org/10.1152/physiolgenomics.00048.2018

Zhang, M., Takimoto, E., Hsu, S., Lee, D. I., Nagayama, T., Danner, T., Koitabashi, N., Barth, A. S., Bedja, D., Gabrielson, K. L., Wang, Y., & Kass, D. A. (2010). Myocardial remodeling is controlled by myocyte-targeted gene regulation of phosphodiesterase type 5. *Journal of the American College of Cardiology*, *56*(24), 2021–2030. https://doi.org/10.1016/j.jacc.2010.08.612

Zhou, Q., Schötterl, S., Backes, D., Brunner, E., Hahn, J. K., Ionesi, E., Aidery, P., Sticht, C., Labeit, S., Kandolf, R., Gawaz, M., & Gramlich, M. (2017). Inhibition of miR-208b improves cardiac function in titin-based dilated cardiomyopathy. *International Journal of Cardiology*, *230*, 634–641. https://doi.org/10.1016/j.ijcard.2016.12.171

SUPPORTING INFORMATION

Additional supporting information can be found online in the Supporting Information section at the end of this article.

How to cite this article: Benkner, A., Rüdebusch, J., Nath, N., Hammer, E., Grube, K., Gross, S., Dhople, V. M., Eckstein, G., Meitinger, T., Kaderali, L., Völker, U., Fielitz, J., & Felix, S. B. (2022). Riociguat attenuates the changes in left ventricular proteome and microRNA profile after experimental aortic stenosis in mice. *British Journal of Pharmacology*, *179*(18), 4575–4592. https://doi.org/10.1111/bph.15910